Plasma Sources Sci. Technol. **16** (2007) R1–R25 doi:10.1088/0963-0252/16/4/R01

TOPICAL REVIEW

A review of recent laboratory double layer experiments

C Charles

Space Plasma, Power, and Propulsion Group, Research School of Physical Sciences and Engineering, The Australian National University, ACT 0200, Australia

E-mail: christine.charles@anu.edu.au

Received 28 April 2007, in final form 2 July 2007
Published 3 September 2007
Online at stacks.iop.org/PSST/16/R1

Abstract
Recent developments in laboratory double layers from the late 1980s to the spring of 2007 are reviewed. The paper begins by a lead up to electric double layers in the laboratory. Then an overview of the main double layer devices and properties is presented with an emphasis on current-free double layers. Some of the double layer models and simulations are analysed before giving a more complete description of current-free double layers in radiofrequency plasmas expanding in a diverging magnetic field. Astrophysics double layers are briefly reported. Finally, applications of double layers to the field of plasma processing and electric propulsion are discussed.

(Some figures in this article are in colour only in the electronic version)

1. Introduction

This review aims to look at experiments on double layers (DLs) that have been carried out since 1985. In essence it is an attempt to provide some continuity to the earlier reviews on DLs (Block 1978, Sato 1982, Hershkowitz 1985, Raadu 1989) and to other specific DL studies (Torven 1979, Levine and Crawford 1980, Carlqvist 1982, Falthammer 2004). Although the primary emphasis is on terrestrial experiments, DLs in space plasmas are described as well as recent modelling and simulation studies. This work clearly concentrates on current-free double layers (CFDL), best known to the author, but for completeness most forms of DLs and applications are mentioned to a greater or lesser degree. The review is not comprehensive and many studies are not reported for lack of space (DLs in tandem mirror devices, in laser devices, ion acoustic DLs). Section 2 presents a lead up to electric double layers in laboratory plasmas. Section 3 reports on double layer devices, properties and their classification. DL models and DL simulations are presented in sections 4 and 5, respectively. Section 6 is devoted to the more recent development of current-free double layers in laboratory radiofrequency plasmas expanding in a diverging magnetic field. Section 7 briefly reports on double layers in astrophysics and is a direct continuation of earlier reviews (Raadu 1989, Falthammer 2004). Finally, section 8 discusses applications of double layers to plasma processing and space propulsion.

2. A lead up to electric double layers in laboratory plasmas

An electric double layer is a narrow localized region in a plasma which sustains a large potential jump, i.e. an electric field. Generally, a low collisional plasma does not sustain electric fields much larger than ambipolar fields except at its boundaries (reactor wall or electrode) where it forms a sheath of potential $V_s \sim (kT_e/e)\ln(M/2\pi m)^{1/2} \sim 5\,(kT_e/e)$ in argon (Lieberman and Lichtenberg 1994), where T_e is the electron temperature, e is the electron charge, k is the Boltzmann constant, and M and m are the positive ion and electron mass, respectively. Following plasma breakdown, the steady-state potential profile near a grounded wall resembles the schematic shown in figure 1 (solid line): in the sheath region, the plasma potential monotonically decreases towards the boundary so as to form an accelerating electric field for the ions and a retarding field for the more mobile electrons, thereby providing equal positive and negative flux at the grounded wall. In the sheath, the ion density is much larger than the electron density and the region is often called a 'single layer' or an 'ion sheath'

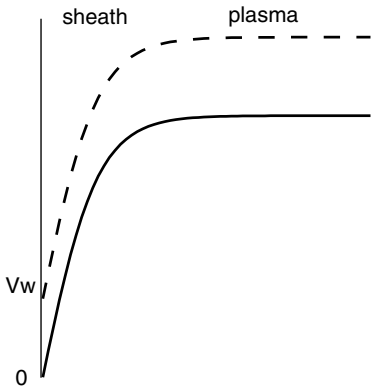

Figure 1. Schematic of a wall sheath potential profile for a grounded wall (solid line) or a floating wall (dashed line).

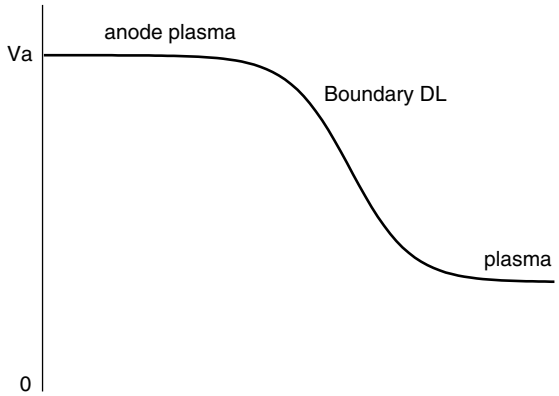

Figure 2. Schematic of an anode double layer (or 'boundary double layer' or 'double sheath') potential profile.

as it contains mostly positive charges. In an argon plasma operating at a pressure of 3 mTorr, kT_e is about 3 eV and the sheath potential is ∼15 V, i.e. close to the ionization energy threshold E_i. In addition, equilibrium of the sheath requires the presence of a presheath region to accelerate the ions to the Bohm velocity $\sqrt{kT_e/M}$ and the corresponding potential drop is ∼0.5–1(kT_e/e) (Lieberman and Lichtenberg 1994, Oksuz and Hershkowitz 2002).

If the wall is left floating, initial plasma conditions may lead to charging of the wall to a positive or negative potential V_w during plasma breakdown and the plasma potential profile will shift up or down accordingly (figure 1, dotted line). If a positive or negative voltage is applied on the wall, defining it as an electrode, the sheath potential profile will be altered as a current can now flow in the external circuit. In dc discharges, the configurations associated with low applied voltages are referred to as anode and cathode sheaths respectively since the structure is still 'attached' to the electrode but with a slightly modified amplitude. For sufficiently high voltages, a plasma will be generated in the vicinity of the anode and the 'sheath' effect described previously will be located at the anode plasma boundary, i.e. away from the anode itself. This stationary 'detached' sheath is defined as a 'double sheath', an 'anode double layer', or a 'boundary double layer'. The schematic of an anode double layer is shown in figure 2: the anode plasma relies on the electrons flowing upstream (towards the anode) with sufficient acceleration to ionize the background gas and

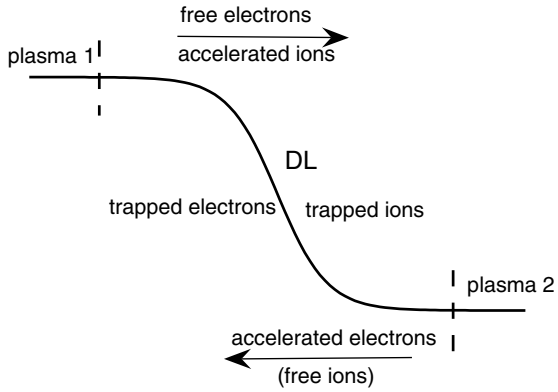

Figure 3. Schematic of potential for a double layer between two plasma sources (grids or aperture as dotted lines) or in an expanding plasma (no dotted lines and plasma 2 = plasma 1). In most cases $kT_i \ll kT_e \ll e\phi_{DL}$ and the free ions term is negligible.

the potential drop of the double layer ϕ_{DL} is somewhat larger than the ionization energy threshold of the gas (E_i), typically 15–20 V in argon. Assuming a symmetry axis halfway in the DL, its structure can be seen as two contiguous sheaths of opposite 'signs', the left one composed of a layer of positive charges (an 'ion sheath') and the right one composed of a layer of negative charges (an 'electron sheath') with a breakdown of quasi-neutrality within the double layer. Similarly to the creation of an anode double layer from an anode sheath, a cathode sheath develops from a negative voltage applied to an electrode and double layers were originally found in front of the cathode in discharge tubes (Hershkowitz 1985). Ionization effects throughout the tube dominated the physics of the DL and its diagnostic was difficult due to the plasma device geometry.

Double or triple plasma devices and single or double-ended Q machines were introduced to allow the control of the particle distribution functions and diagnostic access in a DL region where ionization is not important as the plasma is produced at the end of the discharge rather than throughout the device (Hershkowitz 1985). The separation is indicated by dotted lines in figure 3 and often corresponds to the presence of grids or plates with a small aperture so that most parameters in the target plasma containing the DL can be adjusted. The DL physics studied in those 'flexible' devices forms the largest component of laboratory DLs (Hershkowitz 1985). More recently, two new classes of laboratory DLs have been found in expanding plasmas where the plasma source is the upstream plasma, i.e. plasma 2 in figure 3 is the expansion of plasma 1 and there are no separating grids. Their understanding uses elements drawn from discharge tubes with constriction, anode double layers systems, single to triple plasma device configurations and their properties exhibit similarities with many space plasma DLs.

A recent paper by Hershkowitz (2005) gives an excellent experimental and analytical summary of the knowns and unknowns of sheaths (ion and electron sheaths), presheaths, and sheath-like structures such as double layers. Characterizing a sheath consists of defining its potential $V(x)$ or $\phi(x)$ (the axis perpendicular to the sheath or DL will be noted x or z) and density profiles, its thickness d, and the boundary conditions at the sheath edge (on the plasma side)

such as the electric field and the velocity of incoming particles. Since a DL can be visualized as an adjacent connection of an ion sheath with an electron sheath, identifying the sheath parameters with an emphasis on the boundary conditions at both edges is desirable. In the general case (figure 3), four groups of particles or 'populations' are postulated to maintain the DL (Raadu 1989): a population of trapped (or reflected) low energy electrons on the high potential side of the DL, a population of trapped (or reflected) low energy ions on the low potential side of the DL, a population of high energy electrons which overcome the DL potential barrier and pass from the high to the low potential side of the DL (called passing or free electrons) and a population of high energy ions which overcome the DL potential barrier and pass from the low to the high potential side of the DL (called passing or free ions). The presence of an electron (in most cases but not all) and ion energetic beam on the high and low potential side of the DL, respectively, results from particle acceleration while traversing the DL. These beams may be the first experimental clue to the presence of an electric double layer and these two 'additional populations' (accelerated ions flowing downstream and accelerated electrons flowing upstream) are to be considered along with the passing populations when estimating the net current through the DL (figure 3). A zero net current corresponds to a current-free double layer. All populations will 'interact' with the boundary plasmas and the system's walls. The DL is collisionless and the surrounding plasmas exhibit low collisionality at most. For a full DL description, the plasma boundaries and/or external global current system have to be taken into account, a challenging task. Subscripts 'up' and 'down' will refer to the high and low potential sides, respectively. Subscripts 'e', 'i' and '−' will refer to electron, positive ion and negative ion, respectively.

3. Double layer devices, properties and classification

3.1. (mostly) Current-driven DL devices

3.1.1. Discharge tubes (hot cathode double layer). Double layers were initially found around a hot cathode in a low pressure (about 1 mTorr) mercury arc discharge (Langmuir 1929). The cathode is heated to emit electrons. The maximum electron current is limited by space charge and corresponds to the formation of a second plasma near the cathode and of a doubler layer at this second plasma boundary, often classified as a 'boundary double layer'. The ratio of the electron-to-ion current is equal to $(M/m)^{1/2}$ and is defined as the Langmuir condition. The same current analysis can be done for an anode sheath evolving into an anode double layer. Details on DL experiments in various discharge tube systems can be found in Levine and Crawford's (1980) review. In the presence of a constriction in the gas-discharge tube (figure 4(*a*)), the DL which develops over the cathode side is located at the boundary of the bright 'plasma sac' which protrudes out of the constriction (Andrews and Allen 1971). This DL is not attached to the cathode or anode and is not classified as a 'boundary double layer'. The DL need not be present for the current limitation to occur (Stangeby and Allen 1973). A recent study has investigated the comparison between the case where the cathode is on the constriction side and the case where the anode is on the constriction side (Williamson and Ganguly 2001). In the latter case, neither the 'plasma-sac' nor the double layer is visible and diode-laser absorption measurements of He metastable densities show that the double layer is much weaker. The device consists of a sealed discharge cell filled with He at 1 Torr which includes a Pyrex cell made of two concentric tubes of different diameters.

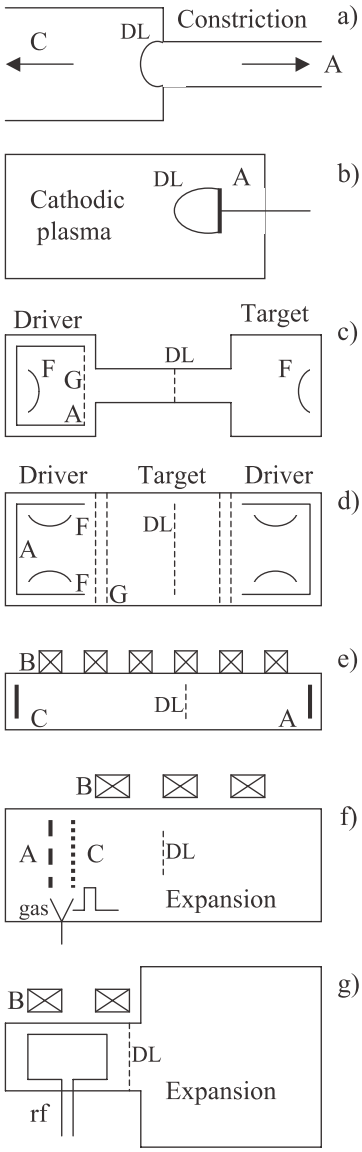

Figure 4. Schematic of the main laboratory DL devices (most common configuration): (*a*) discharge tube with constriction (hot cathode DL), (*b*) anode DL devices, (*c*) double plasma device, (*d*) triple plasma device, (*e*) Q machine, (*f*) two-electron temperature device and (*g*) expansion device (A = anode, C = cathode, G = grid, F = filaments, B = applied dc magnetic field).

3.1.2. Anode double layer devices. When an anode electrode is immersed in a cathodic plasma (figure 4(*b*)), for a sufficiently positive bias voltage, a luminous nearly spherical or cylindrical region ('fireball' or 'firerod') is generated in contact with the anode disc and may develop in multiple concentric DLs (Conde and Leon 1999, Aflori *et al* 2005). The cathodic plasma can be generated using various techniques: a dc arc discharge in mercury vapor at 1 mTorr (Torven and Andersson 1979),

a hot filament discharge in Ar, Kr, or Xe at 0.1 to 2 mTorr (Schrittwieser *et al* 1992, Song *et al* 1991, 1992a), a K^+ plasma column produced using potassium vapour ionized by contact with a heated tantalum plate (Q machine) in a 1 mTorr argon (Song *et al* 1992b) or nitrogen (Barkan and Merlino 1995) background plasma, a radiofrequency inductively coupled hydrogen plasma at a few tenths of mTorr (Tang and Chu 2003). Recent anode DL studies have reported effects of an external magnetic field (convergent, divergent, constant) of various strengths (from 30 to 3000 G at the anode) on the anode DL formation and properties. The field can be constant (50–600 G, Torven and Andersson 1979), divergent with a maximum of 30 G (Schrittwieser *et al* 1992) to 3000 G (Song *et al* 1992b) at the anode or convergent with a minimum at the anode (Tang and Chu 2003). The production of the anode plasma relies on ionization produced by electrons drawn from the plasma to the anode and the DL potential drop must exceed the background gas ionization potential (about 15 V in hydrogen or argon). The anode current voltage characteristic $I(V)$ shows the minimum voltage threshold value for the transition from an anode glow sheath to a stable DL and the characteristic exbihits hysteresis. The latter as well as the thickness of the DL are strongly dependent on the gas pressure and the magnetic field. One- to three-dimensional anode DLs can be created by adjusting the external parameters. The density decreases by a factor of about 2 across the DL. The DL strength and potential steepness increase with the magnetic field for a divergent configuration maximum at the anode. The electrons responsible for the ionization in the anode DL plasma appear as a beam at a mean energy of about E_i in the measured electron energy distribution function (EEDF) upstream (Schrittwieser *et al* 1992). For a B field of 3000 G at the anode, the gradient of the magnetic field is important for determining the position of the double layer (Song *et al* 1992b) over the entire pressure range. However, the DL strength and thickness are not affected by the presence of the magnetic field (Torven and Andersson 1979).

3.1.3. Double and triple plasma devices. Double plasma (DP) devices introduced in the late 1960s (Taylor *et al* 1969) and triple plasma (TP) devices introduced in the late 1970s (Coakley and Hershkowitz 1979) consist of one grounded 'target' chamber (usually non-magnetized) where the DL forms and one or two biased 'driver' chambers, respectively. The two plasma sources (target and driver for DP (figure 4(*c*)), two drivers for TP (figure 4(*d*))) are usually hot filament produced plasma discharges operating with inert gases (He, Ne, Ar, Kr, Xe). Typical parameters in argon are $n_e \sim 10^7$–$10^{10}\,\mathrm{cm}^{-3}$, $T_e \sim 10\ T_i \sim 2\,\mathrm{eV}$ for a pressure range 0.01–1 mTorr. Grids separating the electrically independent chambers are used.

In a DP device (figure 4(*c*)) an ion beam of well defined energy is injected from the driver into the low density partially ionized target plasma (Johnson *et al* 1989) and a DL with $(e\phi_{DL}/kT_e) \sim 5$–10 forms when the electrons from the target plasma are not sufficient to neutralize the injected ion beam. The position of the DL is close to that defined by the Langmuir condition and depends on the external parameters (discharge currents, target chamber pressure, axial magnetic field strength if any). The injected species can be an electron beam (Quon and Wong 1976). Recent studies in DP devices include magnetic field studies and ionization instabilities studies (Johnson *et al* 1989, 1990).

In a TP device (figure 4(*d*)) up to four grids are used to control the plasma potential and particle distribution functions at the DL chamber boundaries and an extended range of DL strength $(e\phi_{DL}/kT_e) \sim 1$–14 can be obtained (Hershkowitz 1985). To limit ion–neutral collisions in the DL chamber, the pressure is kept below 1.3 mTorr and the electron density and temperature are in the 10^6–$10^9\,\mathrm{cm}^{-3}$ and 1–4 eV ranges, respectively, in argon. In the 1980s, TP devices have been very successful in determining a large core of DL physics in the laboratory (Hershkowitz 1985, Hollenstein *et al* 1980). Similar DP and TP configurations can be obtained by using apertures rather than grids (Torven 1982, Torven *et al* 1985, Merlino and Loomis 1990). Filamentary DLs have been studied in TP devices using a variable aperture (Theisen *et al* 1994). The plasma source can be a heated cathode plasma column rather than a hot filament discharge (Plamondon *et al* 1988, Lindberg 1992, Volwerk 1993).

3.1.4. Single-ended and double-ended Q machines. Similarly to DP and TP devices, in Q machines (figure 4(*e*)) the plasma is produced at one end (single-ended) or two ends (double-ended) of the system rather than throughout the device so that ionization is not important in the DL region (Sato *et al* 1981, 1986, Izuka *et al* 1982, Sato 1982). Typical operating pressure in the vicinity of the DL is less than 0.8 mTorr. The plasma is usually produced by contact ionization of potassium or sodium atoms on a hot tantalum plate which is biased. The radius of the plate determines the radius of the column and is usually small (less than 10 cm). In the double-ended Q machine, the DL is generated by applying a potential difference between the two hot plates or by using grids of variable shapes and biases in between the end plates (Kuhn 1979). The plasma parameter ranges associated with Q machines are radically different from those corresponding to all other devices: a strong axial dc magnetic field (2–4 kG) is applied, both the electron and ion Larmor radii are much smaller than the plasma radius and the plasma is fully ionized ($n_e \sim 10^{12}\,\mathrm{cm}^{-3}$, $kT_e \sim kT_i \sim 0.1\,\mathrm{eV}$). The second plasma source can be an argon discharge produced between a mesh anode and an oxide cathode (Hatakeyama *et al* 1983).

3.1.5. Current-free operation of Q machines and TP devices. Subsequent to Perkins and Sun's theoretical prediction of current-free DL solutions (Perkins and Sun 1981), current-driven discharges were set up without any current flowing through the external system: the DL could be maintained with similar grid potentials in a TP device (Chan *et al* 1981) and in the absence of any externally applied potential difference between the two plasmas in a double-ended Q machine (Hatakeyama *et al* 1983). Two new classes of current-free DLs were subsequently detected in expanding plasmas (Hairapetian and Stenzel 1990, Charles and Boswell 2003).

3.2. (mostly) Current-free DL devices

3.2.1. Two-electron-population expanding plasma device. Hairapetian and Stenzel (1988) reported on the expansion of a two-electron-population argon plasma (figure 4(*f*)) of density

about 10^{11} cm^{-3} into vacuum along an axial magnetic field (30–50 G). The electron distribution consists of a Maxwellian ($kT_e \sim 3$–5 eV) and an energetic tail (5% at 80 V) created by injecting a pulsed (1 ms 'on') collimated neutral argon beam at 0.5 mTorr into a region containing a filamentary grounded cathode and a grid anode separated by 0.7 cm. The pulsed discharge plasma resulting from ionization of the neutral beam by the 80 V/8 A discharge electrons (emitted from the cathode) expands in the high-vacuum chamber and reaches the end wall in 100 μs. During the one-dimensional expansion, a DL (with zero net current) or rarefaction shock forms and propagates as a result of the separation between the hot and cold electrons: the low potential side at the expansion front contains mostly hot electrons while the high potential side (near the plasma source) contains both the tail and cold electrons. Ion acceleration and the formation of an ion beam is measured using an energy analyser. Some ions acquire an energy above that of the energetic electron tail. An ion density decrease is observed in the vicinity of the current-free propagating DL. No DL is observed at background pressures above 2×10^{-5} Torr and a necessary condition is the absence of any ionizing or charge exchange collisions in the expansion region. In subsequent experiments (Hairapetian and Stenzel 1990, 1991) the propagating DL becomes a stationary DL from 200 μs till the end of the 1 ms discharge and the DL can be characterized as a weak current-free magnetic field aligned DL with $e\phi_{DL} \sim kT_e$, where T_e is the temperature of the 'free' electron population ($kT_e \sim 30$ eV). The estimated thickness is 50–100 Debye lengths and there is no electron beam upstream. The DL can be sustained with a current. There are no stationary ions downstream, only the ion beam formed by acceleration in the DL potential drop. The DL occurs at the position where the density of the tail electrons exceeds that of the Maxwellian electrons.

3.2.2. Current-free expanding devices. Recently a new class of CFDLs has been diagnosed in laboratory radiofrequency (13.56 MHz) plasmas (Charles and Boswell 2003, Cohen *et al* 2003, Sun *et al* 2005, Plihon *et al* 2005a, 2005b, 2007, Sutherland *et al* 2005, Corr *et al* 2006, West *et al* 2007). The plasma source is usually a helicon source which can be operated in capacitive, inductive or wave coupling mode (figure 4(*g*)). This stationary DL spontaneously forms in the current-free plasma expansion in a divergent magnetic field for low operating gas pressures (less than 2 mTorr) and for a variety of electropositive (Ar, He, Xe) or weakly electronegative gases (H_2, O_2). The DL does not necessarily need to be current-free as a source terminated by a dc connection to ground or a biased plate also exhibits the presence of the DL (Cohen *et al* 2003, Meige *et al* 2005a, 2005b, Plihon *et al* 2007). This expanding DL is described in detail in section 6. A variety of recent configurations of plasma expansion from a variety of plasma sources has been diagnosed, some with the presence of a CFDL and others without: expansion from a small diameter helicon (Shamrai *et al* 2006) or inductively coupled plasma (Popescu *et al* 2006) source, or from an electron cyclotron resonance (Aanesland and Charles 2006) or an annular inductively coupled plasma (Volynets *et al* 2006) source. Interestingly, the last two cases do not exhibit a double layer: the plasma parameters measured along the expansion are surprisingly similar and exhibit a strong gradient in electron temperature and very negative floating potentials. The CFDL detailed in section 6 is associated with positive floating potentials in the plasma source.

3.2.3. Electronegative double layer devices. Experimental evidence of DLs in a plasma with negative ions was shown in a TP device (Merlino and Loomis 1990). The effect of the negative ions was to lower the DL potential drop and to generate the formation of a second double layer further downstream. The location of the DLs could be changed by varying the external plasma parameters. In the expanding plasma system described in the previous subsection, but in the absence of the diverging magnetic field, a DL may form in a very electronegative plasma (SF_6, SF_6/Ar) under specific experimental conditions (Plihon *et al* 2005a, 2005b, Plihon 2006) and its properties differ from those corresponding to the electropositive gases. In the magnetic field free expansion region of an inductively coupled electronegative SF_6/Ar plasma (typically at 1 mTorr with $n_e \sim 10^{11}$ cm^{-3}, $kT_{e\ up} \sim 4.5$ eV and $kT_{e\ down} \sim 3$ eV), the DL formation requires a certain fraction of negative ions: for SF_6 concentrations in between 8% and 13%, a stationary DL (with $(e\phi_{DL}/kT_e) \sim 1.5$) forms at the junction between the plasma source and the diffusion chamber which separates a high electronegativity ($(n_-/n_e) \sim 12$) plasma downstream and a low electronegativity ($(n_-/n_e) \sim 2$) plasma upstream. For high SF_6 concentrations a downstream instability is observed which relates to the periodic formation and propagation of the DL. The large fraction of negative ions just downstream are accelerated towards the plasma source and the DL is 'crossed' by two ion beams of opposite charges in opposite directions (Plihon *et al* 2005a, 2005b). The spherical shape of the DL is visible and used for the modelling (Chabert *et al* 2006). The DL propagates from the end of the source tube to the end of the expansion region with a velocity of 150 m s^{-1} and its potential drop decreases during the propagation. A new DL forms before the end of the expansion region is reached. Adding a static axial magnetic field reduces the electronegative DL parameter range and leads to a radially stratified plasma with a low electronegativity central column encapsulated within a high electronegativity ion–ion annular discharge (Corr *et al* 2006). This stratification with the presence of an applied axial magnetic field has been observed in similar inductive systems in plasmas with low electronegativity (Charles and Boswell 1995a).

3.2.4. Astrophysics double layers. DLs occur 'naturally' in our cosmic habitat. The closest region of interest is the auroral cavity at the ionosphere–magnetosphere boundary above the North and South poles of the Earth. Strong magnetic field aligned DLs with various properties form in this cavity. The DLs have been characterized in passive experiments using probes on satellites such as FAST (Ergun *et al* 2001, 2002) or in active experiments associated with the injection of barium jets (Wescott *et al* 1976, Block 1978).

3.3. DL properties and classification

The large number of DL device configurations and associated DL properties make a classification difficult and possibly

Table 1. Summary of the main parameters in DL laboratory devices.

DL Device	Gas/ion	p (mTorr)	B (G)	n_e (cm^{-3})	T_e (eV)	T_i (eV)	ϕ_{DL} (V)	$e\phi_{DL}/kT_e$
Discharge tube	Hg	∼1	0	10^{10}–10^{11}	2–10	≪0.2	15–30	5–10
Anode DL	Ar^+	∼1	0–3000	10^9–10^{10}	0.2–2	⩽0.2	15–20	5–10
Double plasma	Ar^+	0.01–2	0–200	10^6–10^{10}	2	⩽0.2	15	1–10
Triple plasma	Ar^+	0.01–1	0–360	10^6–10^9	2	0.2	5–1000	1–14
Q machine	K^+	⩽1	2000–4000	10^{12}	0.1	0.1	5–400	1–2000
Two Te expansion	Ar^+	⩽0.02	30–50	10^9–10^{11}	3/30 (tail)	0.8	∼30 (tail)	1
Expansion	Ar^+	0.2–2	⩾50	10^9–10^{12}	⩾3	0.2	10–100	2–7
Auroral cavity	H^+ and O^+	—	10^{-4}–0.1	1–10^5	500–0.2	—	10^3–10^4	—

erroneous in some aspects. Nevertheless an attempt is made here to establish a quick guide to the main DL devices, external parameters and essential plasma and DL parameters (table 1). In most cases, the plasma on either side of the DL is collisionless or exhibits low collisionality and the operating pressure is less than 2 mTorr (exceptions to this can be found in Williamson and Ganguly (2001) and Plihon *et al* 2005b). A DL is defined as weak if $(e\phi_{DL}/kT_{fe}) < 10$ and strong if $(e\phi_{DL}/kT_{fe}) \geqslant 10$, where T_{fe} is the free electron temperature, i.e. the electron temperature on the low potential side of the DL. Single double layers can evolve into stair-step (multiple) DLs (Chan and Hershkowitz 1982, Diebold *et al* 1992, Intrator *et al* 1993). In the laboratory, ionization in the plasma sources is typically ionization of low pressure mercury vapour, contact ionization on a hot plate in potassium vapour, ionization by electrons emitted from heated filaments or an applied voltage on an immersed electrode generating secondary electron emission, or inductive rf coupling with an antenna wrapped around a tube. Although not always a necessary condition for the existence and stability of a DL, the presence of an externally applied axial magnetic field will affect the particle dynamics and consequently some aspects of the DL such as its location in the device. Most devices not requiring the presence of an applied magnetic field (DL device, anode DL devices, TP devices) have been recently set up with a magnetic field to get more insight into DLs occurring in astrophysical plasmas. Except for a strongly electronegative DL, all recent CFDL systems with plasma expansion are associated with a magnetic field of moderate strength (50–300 G). The shape of the DL is often associated with the geometry of the device (from planar, to rod, to spheres, to U-shapes) and with the magnetic field configuration. The electron density range often results from the type of plasma source and applied external parameters and DLs can be formed for an extended range of densities (table 1). Most laboratory devices generate weak DLs where $kT_e \sim 10\ kT_i \sim 1$–5 eV. DL strengths up to 14 have been reported in the triple plasma device (Coakley *et al* 1978). Magnetic fields of a few kG are always present in Q machines and $kT_e \sim kT_i \sim 0.1$ eV leading to strong DLs.

4. DL models

DLs must fulfil three conditions (Block 1978): a potential drop larger than T_e, an electric field stronger in the DL than outside and a global zero charge of the DL (quasi-neutrality is locally violated at the position of the DL). Modelling a steady-state DL potential structure in 1D necessitates solving the time independent Vlasov equation and Poisson's equation and implementing the charge neutrality and zero electric field conditions at the DL boundaries. The mathematical representation is non-linear and solutions cannot easily be derived. The broad range of DL properties have led to the development of various models (Raadu 1988, 1989, 1994). The present section is not intended to be comprehensive but to give an overview of modelling methods of interest to the experimentalist and to provide some basis for further development of CFDL models. The low and high potential sides of the DL are referred to as downstream and upstream, respectively.

4.1. BGK procedure (three to six groups of particles)

In 1957 the existence of a class of solutions to the Vlasov equations 'containing' potential structures associated with non-linear electrostatic waves, known as the BGK solutions was reported (Bernstein *et al* 1957). This approach was subsequently used (Knorr and Goertz 1974) by predetermining a steady-state DL potential profile $\phi(x)$ and then solving the time-independent Vlasov–Poisson equations by adjusting the distribution function of one of the particle populations, in that case the trapped electrons, for given distributions for the other three groups of particles (accelerated electrons and ions, and trapped ions). The distribution function for any free or trapped particle of mass and charge m_j and q_j is expressed as a function of the energy W:

$$W = \tfrac{1}{2}m_j v^2 + q_j\phi(x). \tag{1}$$

Poisson is then written as

$$\epsilon_0\frac{\mathrm{d}^2\phi(x)}{\mathrm{d}x^2} = -\sum_j q_j\int_{W_{j1}}^{W_{j2}}\frac{f_j(W)\,\mathrm{d}W}{\sqrt{2m_j(W-q_j\phi(x))}}, \tag{2}$$

where W_{j1} and W_{j2} are the energy limit of particle j (ϵ_0 is the permittivity of free space). Multiplying by $\mathrm{d}\phi(x)/\mathrm{d}x$ and integrating with respect to x yields the differential equation:

$$\frac{1}{2}\epsilon_0\left(\frac{\mathrm{d}\phi(x)}{\mathrm{d}x}\right)^2 + V(\phi) = \text{const}, \tag{3}$$

where the potential term is referred to as the Sagdeev potential (Raadu 1989):

$$V(\phi) = -\sum_j q_j\int_{W_{j1}}^{W_{j2}} f_j(W)\,\mathrm{d}W\sqrt{2m_j(W-q_j\phi(x))}. \tag{4}$$

This potential must satisfy the DL boundary conditions. Determining the particle distribution functions in the laboratory and in space is exceedingly difficult and it is often

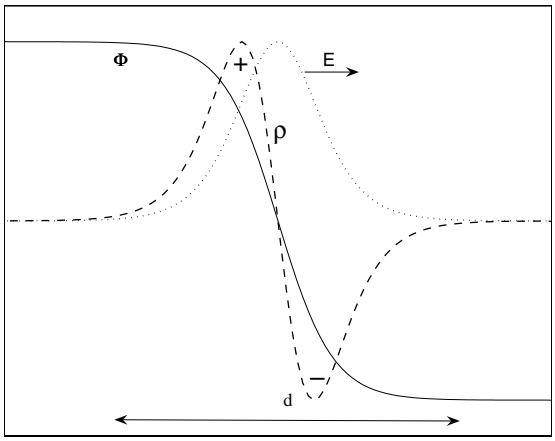

Figure 5. Schematic of a weak double layer potential (solid line), electric field (dotted line) and charge density (dashed line) profiles (the solution exhibited is $-\tanh(x/2)$ for x from -10 to 10 and d is the DL thickness).

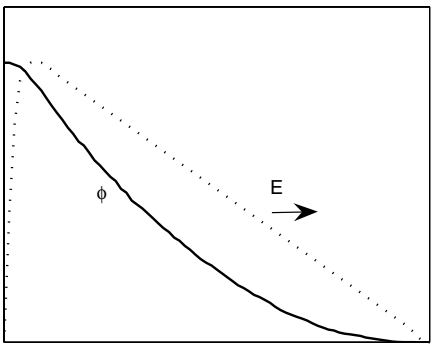

Figure 6. Schematic of a strong relativistic double layer potential (solid line) and electric field (dotted line) profiles.

not possible to express the Sagdeev potential. For weak DLs, it can be expanded in powers of ϕ

$$-V(\phi) = A_1\phi^2 + A_2\phi^3 + A_3\phi^4 \tag{5}$$

leading to a typical DL solution of equation (3) in the form

$$\phi(x) = -\frac{1}{2}\left(\frac{A_2}{2A_3}\right)\left(1 - \tanh\left(\frac{x - x_0}{d}\right)\right) \tag{6}$$

rewritten as

$$\phi(x) = \phi_{\mathrm{DL}}\left(1 - \tanh\left(\frac{x}{d}\right)\right), \tag{7}$$

which leads to a sketch of the potential, charge density and electric field shown in figure 5 (d is the DL thickness). The potential is prominently symmetric, a characteristic of weak non-relativistic DLs of plane structure, with similar width for the adjacent positive and negative space charges (Hershkowitz *et al* 1981, Carlqvist 1982). Strong relativistic DLs such as many DLs in astrophysics are unsymmetrical (Carlqvist 1982) with a sharp increase of the electric field on the positive side followed by a gradual decrease over most of the DL width (figure 6). Electrostatic potential troughs (i.e. a combination of several opposing DLs) are generally required for a self-consistent BGK equilibrium (Block 1978). The BGK approach has been successfully applied to the triple plasma device DL where the distribution functions are accurately measured and controlled and a self-consistent solution has been numerically found. In other instances, a pre-determined potential such as that in equation (7) is imposed to obtain information on distribution functions. Other information such as the Langmuir condition, the Bohm criterion may be derived or discussed from boundary condition requirements without solving the equations. Although the BGK procedure can be used by including an unlimited number of distributions, the most common cases deal with 3–6 distributions. Stationary solutions of the Vlasov–Poisson system in BGK DL models may be derived analytically or numerically. However, the stability of the solutions cannot be determined.

4.1.1. Application to the triple plasma device DL (four distributions). The BGK procedure has been successfully used (Hershkowitz *et al* 1981) to model the triple plasma device DL. The range of energies for each group of particles (figure 3) is known and the density is given (Knorr and Goertz 1974) by integration over each range using

$$n_j(x) = N\sqrt{\frac{m_j}{2\pi T_j}}\int_{W_{j1}}^{W_{j2}} \frac{\mathrm{e}^{-(W - q_j\phi(x))/T_j}}{\sqrt{2m_j(W - q_j\phi(x))}}\mathrm{d}W$$
$$= n_j[\phi(x)]. \tag{8}$$

Boundary conditions consistent with the experiment are implemented and similar electron temperatures are considered for the two plasma sources. The trapped distributions are assumed Maxwellian and the accelerated particles enter the DL at their thermal speed (Bohm sheath neglected in the plasma sources). Two non-linear equations are solved numerically to obtain the plasma potential and density profiles within the DL, as well as the total charge density profile. The total ion and electron density profiles show similar densities on either side of the DL but a dip inside the DL. The respective dips are shifted in position and result in the two adjacent layers of similar width but opposite charges which form the weak DL (figure 5). The Langmuir condition is discussed and it is shown that it does not need to be satisfied for weak double layers. The model of the well diagnosed experimental triple plasma device DL is complete and self-consistent. For space DLs, and expanding DLs, there are often many unknowns and such a complete treatment cannot easily be obtained.

4.1.2. DL model in multispecies plasma. The existence of weak DLs based on the analytical expansion of the Sagdeev potential (equation (5)) is discussed by Verheest and Hellberg (Verheest and Hellberg 1997). DLs cannot be supported by only one Boltzmann and one cold fluid species. At least two thermal species must exist which can be described by a Boltzmann distribution or retain finite-mass effects. The Sagdeev potential is derived for multispecies plasmas such as electronegative plasmas. It is found that any DL behaviour is excluded except for some soliton solutions. A model of the experimentally characterized electronegative double layer in the expanding region of an inductively coupled plasma has been recently reported (Chabert *et al* 2006) in which an upstream plasma model is coupled to a downstream plasma model via the DL. The DL potential drop (∼7 V) is calculated as a function of the operating pressure (0.6–3 mTorr). More recently, a full self-consistent hybrid model of the propagating DLs has been developed which calculates the electron energy

distribution function, the electron temperature and the various source terms (Meige *et al* 2007).

4.1.3. Perkins and Sun's model (not BGK). In principle, a DL can exist without any net current (Block 1978). Perkins and Sun (1981) predicted current-free solutions to a 1 D Vlasov–Poisson plasma where the trapped ion density downstream (governed by the parameter Δ) and the DL potential drop ϕ_{DL} are the two components of a non-linear two-component eigenvalue problem which determines the DL solution. Upstream the plasma has Maxwellian distributions for electrons and ions with distinct temperatures (T_e, T_i). Δ and ϕ_{DL} are plotted versus T_e/T_i ranging from 0.1 to 10. For a T_e/T_i ratio of 10, $e\phi_{DL}/kT_e$ is about 1.1. Δ determines the trapped ion density, hence where the DL occurs. If the correct value of Δ exists within a plasma, then the DL occurs at that point. Hence forced changes in the distribution functions may result in DL formation and these distributions need not carry current.

4.1.4. Two-electron-temperature plasma current-free DL model (not BGK). Analytical modelling of the experimental two-electron-population CFDL (figure 4(f)) has been reported (Sato and Miyawaki 1992). The model assumes a collisionless plasma in a 1D planar geometry with absorbing and electrically floating walls. In the model, a small number of cold ions produced on the low potential side are present. For low hot/cold electron density ratios, a monotonically decreasing potential structure composed of the 'first' presheath (high potential region), a CFDL, the 'second' presheath (low potential region) and the wall sheath is found. The DL potential drop is of the order of the 'effective' temperature of the energetic electrons. The DL thickness is about 50 Debye lengths and the position of the DL depends on the location of ionization of the gas in the upstream region. Charging of the wall to positive values is found which accommodates the development of large plasma potentials in the 'first' presheath.

4.1.5. Neutron star current-free DL model (six distributions). Accretion onto neutron stars with the presence of a current-free double layer in a magnetized plasma is reported in section 7. A model is developed (Williams *et al* 1986) with an analytical form of the potential in the form of equation (7). Six groups of particles (accreting (N_3,N_2), atmospheric (N_5,N_1) and trapped (N_4,N_6) protons and electrons, respectively) are described using four types of distributions: half Maxwellian, full Maxwellian, waterbag, or a superposition of waterbag and Maxwellian. The Vlasov equation is solved for each group of particles to determine the distribution function at arbitrary x. Poisson's equation is expressed as

$$\frac{A}{4\pi e}\frac{d^2V(x)}{dx^2} = N_1(x) + N_2(x) - N_3(x) - N_4(x) - N_5(x) + N_6(x), \quad (9)$$

where A is the area of the accretion column. Assumptions are made on five of the distributions to determine the density of the sixth distribution (trapped electrons N_6) consistent with the potential $V(x)$. A zero net current is imposed as well as boundary conditions relevant to the accretion column. In this model, the BGK approach leads to some qualitative indication on the viability of the current-free double layer concept for the deceleration mechanism of the accreting matter.

4.2. Langmuir's 'double sheath' model (two groups of particles)

In 1929, Langmuir first described a DL formed between an electron emitting cathode (low potential side) and an ion emitting anode (high potential side) with an applied dc voltage across the gap (Langmuir 1929). Langmuir's 'double sheath' model includes two groups of particles only, the accelerated electrons flowing to the anode and the accelerated ions flowing to the cathode and assumes that the particles are mono-energetic with zero incident velocity at the DL boundary. The variation of potential inside the DL is assumed monotonic, zero electric field is implemented at the boundary and magnetic effects, collisions and ionization in the DL are neglected. Energy conservation inside the DL for the two groups of particles is applied and used to calculate the total charge. Poisson's equation is integrated once to express the electric field where the constant of integration is found by using the boundary condition at the low potential side ($E = 0$ at $V = 0$). Subsequently implementing the high potential side boundary condition ($E = 0$ at $V = V_{DL}$) leads to the Langmuir condition:

$$I_e/I_i = (M/m)^{1/2}, \quad (10)$$

where I_e and I_i are the electron and ion current flowing across the gap, respectively. The electron current density drawn across the DL is limited by the ion current density flowing in the opposite direction. The model is not physically self-consistent as it predicts infinite space charges at the DL boundaries. A second integration of Poisson's equation to obtain $V_{DL}(x)$ is not discussed. The 1929 Langmuir condition is the non-relativistic limit of a more general condition derived for strong relativistic double layers (Carlqvist 1982):

$$I_e/I_i = \left(\frac{\phi_{DL} + 2mc^2/e}{\phi_{DL} + 2Mc^2/Ze}\right)^{1/2}, \quad (11)$$

where c is the velocity of light and Ze is the ion charge. This condition has been widely tested by experimentalists operating current-driven DL discharges and most models 'refer' to the Langmuir condition by evaluating its validity over various parameter ranges. For weak DLs this condition is not always verified (Hershkowitz 1985, Lieberman *et al* 2006).

4.3. Double sheath between two-plasmas model (four groups of particles).

Andrews and Allen (1971) obtained conditions to embed a DL in a quasi-neutral plasma using the four following groups of particles, thermal ions, accelerated ions flowing downstream, accelerated electrons flowing upstream and thermal electrons. This corresponded to the discharge tube with constriction experiment, where upstream is the constricted side (figure 4(a)). For assumed mono-energetic accelerated species and Maxwellian thermal species, they determined the density ratios of the species at each edge of the DL, as well as the velocities required for the accelerated species entering a given DL potential drop. The latter corresponds to

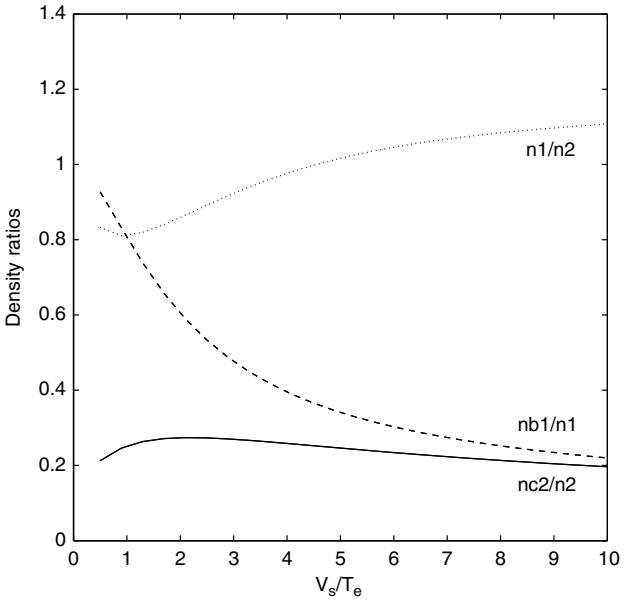

Figure 7. Results from the CFDL model (Lieberman and Charles 2006, Lieberman *et al* 2006): n_1/n_2 (dotted line), n_{c2}/n_2 (solid line), and n_{b1}/n_1 (dashed line) density ratios versus double layer strength V_s/T_e; n_1 and n_2 are the total density just downstream and upstream of the DL, respectively; n_{c2} is the density (at the upstream boundary) of accelerated electrons flowing upstream and n_{b1} is the density (at the downstream boundary) of accelerated ions flowing downstream.

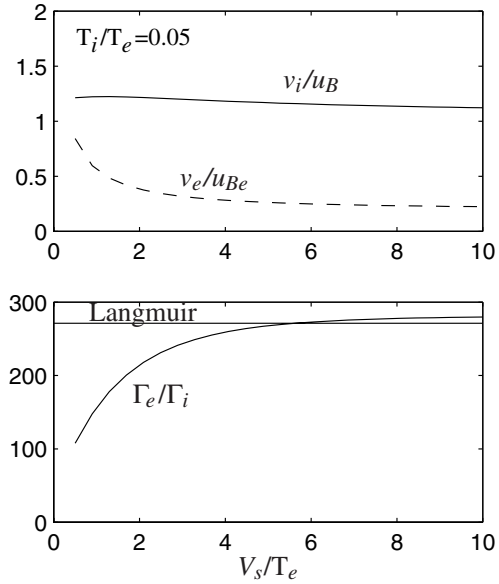

Figure 8. Results from the CFDL model (Lieberman and Charles 2006, Lieberman *et al* 2006): (top panel) ion velocity v_i (solid line) and electron velocity v_e (dashed line) entering the double layer versus V_s/T_e; the ion velocity is normalized to $u_B = (kT_e/M)^{1/2}$, and the electron velocity to $u_{Be} = (kT_i/m)^{1/2}$; (bottom panel) the ratio of electron-to-ion flux for the accelerated species versus V_s/T_e; the Langmuir condition (equation (10)) is shown as the solid horizontal line.

'pre-acceleration' in a 'pre-sheath' region on each side of the DL. This was also reported by Block (1972) for strong DLs and can be defined as the 'Bohm criterion' for DLs. The basic procedures are those used by Montgomery and Joyce (1969) to describe laminar shocks.

4.4. Current-free double layer model (five groups of particles)

Modelling work has been initiated to model the recently diagnosed helicon CFDL: it is first assumed that a DL of potential V_s (V_{DL} called V_s in the model) forms at the junction between a downstream region 1 and an upstream region 2 at $z = h$ cm and the length and diameter of the two regions are inputs to the model (subscripts 1 and 2 refer to the downstream and upstream double layer edges, respectively). Andrews and Allen's procedure (Andrews and Allen 1971) is followed (subscripts a, b, c and d refer to thermal ions, accelerated ions, accelerated electrons and thermal electrons, respectively), but two implementations based on experimental results are made. An initially near-half Maxwellian, rather than mono-energetic, accelerated electron group is introduced. This leads to the inclusion of a fifth species upstream in the form of an accelerated electron group originating from the near-half Maxwellian accelerated electrons and reflected from the end wall of the source region (high potential). This 'counter-streaming' or 'reflected' electron population group contributes exactly the same charge density to the DL and to the downstream plasma as the original group (near-half Maxwellian) hence making no distinction between current carrying and CFDL. Figure 7 shows the modelled density ratios as a function of V_s/T_e (T_e in volts in the model). The ratio of total downstream-to-upstream density (n_1/n_2) (dotted line) is nearly unity over the entire range of DL strengths. The accelerated electrons (solid line) comprise about 20% of the total density at the upstream edge of the DL. The accelerated ions (dashed line) over the total downstream density ratio decreases with increasing DL strength. Figure 8 shows the entering ion and electron velocity ratios and flux ratio as a function of V_s/T_e for a given T_i/T_e of 0.05. The accelerated ions enter the DL at 1.2–1.3 times the Bohm velocity and the Langmuir condition (solid horizontal line) is not verified for DL strength below 5. The DL solution to Andrew and Allen's procedure provides information on the existence or not of a DL solution and on density ratios and entering velocity ratios at the DL boundary for a given DL potential drop. It does not lead to the absolute value of the DL potential drop. This is obtained in the CFDL model by determining particle balance in the upstream and downstream plasmas embedding the DL. The downstream particle balance from low pressure diffusion theory in an unmagnetized plasma is used to obtain T_e for a given gas pressure and T_e is assumed constant along the z-axis. The upstream particle balance is then used to numerically obtain the absolute value of the DL potential drop. The upstream particle balance is strongly influenced by the introduction of the fifth species, the near-half Maxwellian shifted by an energy corresponding to that of the DL potential drop and representing the accelerated electron group upstream, which provides an additional ionization term. The relative density profile along z is obtained downstream and upstream of the DL. The absolute potential profiles on axis are obtained by setting the zero potential at the downstream wall and an associated floating potential of $\sim 5\, kT_e$ across the sheath (both verified experimentally). The potential drop across the sheath at the upstream floating wall is obtained by equating the

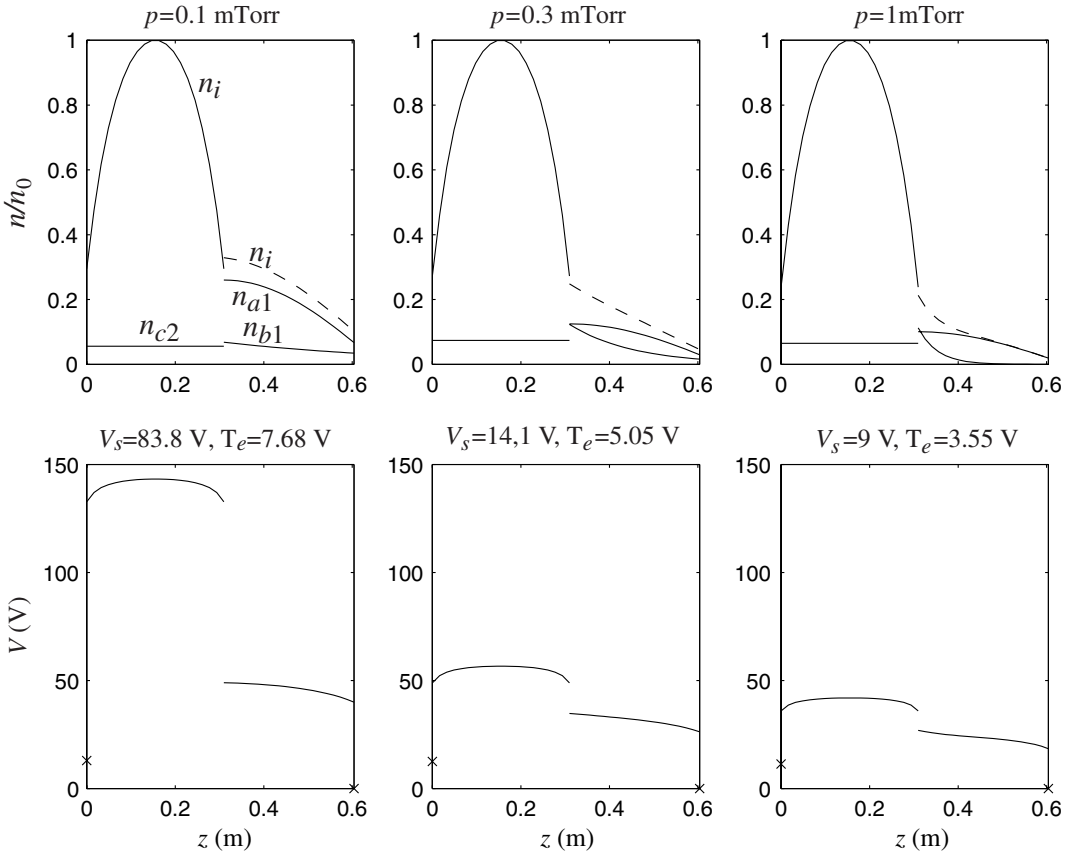

Figure 9. Results from the CFDL model (Lieberman and Charles 2006, Lieberman *et al* 2006): Potential V and total ion density n_i versus position z at (left panels) 0.1 mTorr, (middle panels) 0.3 mTorr and (right panels) 1 mTorr; the downstream total density (dashed) is decomposed into the accelerated ion beam density (decaying exponential n_{b1}, solid) and the thermal ion density (n_{a1}, solid); n_{c2} is the density of accelerated electrons flowing upstream; the wall potentials V_w are given by the crosses (12 V at 0.2 mTorr).

ion and electron fluxes and along with the plasma potential calculated near the wall is used to deduce the floating wall potential V_w. Examples are given in figure 9 for three operating pressures. The model is self-consistent and is compared with the experiment in section 6.7.

4.5. Analytical studies of CFDLs with magnetic field

A recent analytical derivation of a plasma expansion in a diverging magnetic field based on classical sheath theory (Chen 2006) shows that an ion sheath must form within the plasma at a position where the plasma radius has expanded by 28%, with the only assumption being of Maxwellian electrons. At this position the ions have reached the Bohm velocity and an ion sheath or single layer forms. Following the usual sheath theory (Lieberman and Lichtenberg 1994, Chen 2006), the ion sheath potential builds up to the energy-limited sheath drop of about 5 (kT_e/e) in argon. It is suggested that this sheath or single layer evolves into a double layer (Chen 2006).

Momentum considerations in a collisionless-plasma DL configuration has been treated theoretically (Fruchtman 2006) using a waterbag distribution for the trapped particle populations (figure 3), for strong asymmetrical DLs (such as at the aurora cavity-ionosphere boundary) and for symmetrical DLs. It is found that the electric field in the DL does not impart momentum to the particles. A second analysis of plasma flow in a varying cross section $A(z)$ (such as the converging-diverging magnetic field configuration of a Laval nozzle, or the diverging-only configuration of an expanding rf plasma) is carried out with the assumption of the electron density and electric potential obeying the Boltzmann relation. For no potential difference between the two opposite plasma edges (no current) and a plasma generated near the maximum B field (minimum $A(z)$), a cross section increase by a factor of 10 leads to a Mach number of 2 and a gradual potential decrease by a factor of 2.5. The scale length of the decreasing B field dictates that of the potential. In this CFDL, the magnetic field force is the source of plasma thrust, not the electric field pressure (section 8).

5. Double layer simulations

The kinetic properties of DLs can be very effectively studied by numerical simulation over a computational grid (Sulkanen and Borovsky 1992, Singh and Khazanov 2003). Such simulation should determine whether the analytical BGK solutions (if they can be derived) are stable. If a stable DL is obtained, the electrical potential, electric field (hence DL strength and thickness), electron and ion velocity phase space are obtained along the 'simulated grid' (z in 1D) and instabilities in these parameters may be observed and studied. In this section two inherently different recent simulations are discussed: a Vlasov

simulation (with BGK initialization) of the DL between the ionosphere and the auroral cavity and a fully self-consistent particle-in-cell (PIC) simulation of the recently observed laboratory current-free DL (section 6).

5.1. Vlasov simulation with BGK initialization

Strong current-driven DLs can be modelled by 1D open boundary Vlasov simulations (Newman *et al* 2001). In a Vlasov simulation with BGK initialization of the auroral upward-current region (Main *et al* 2006) a monotonic mapping between the potential ϕ and z is assumed as well as the initial upstream and downstream distributions (based on the FAST satellite data) of the electrons and ions (H^+ and O^+). A pseudopotential method is used to find $z(\phi)$ which is inverted to find $\phi(z)$ and map the distributions ($f(\phi(z), v_z) \rightarrow f(z, v_z)$) used to seed the Vlasov simulation. The aim is to find candidate distribution functions that self-consistently support the parallel electric field of a DL. Open boundaries (no sheath build-up) are imposed at both ends. As such, the treatment is that of the DL itself, not of the DL embedded in the ionosphere and auroral cavity plasmas. Features seen in satellite observations such as parallel electric fields, particle distributions, ion phase space holes and wave turbulence are well reproduced in the simulation.

5.2. Particle-in-cell simulation of CFDL

The first numerical simulation of a plasma double layer was reported in 1975 (Goertz and Joyce 1975). Recently a PIC simulation of the experimental CFDL has been reported (Meige *et al* 2005a, 2005b, Meige 2006, Sun *et al* 2005). For a PIC simulation to self-consistently produce a 'free' standing DL, the properties of the computational grid boundary need to be specified. If the grid encompasses the DL and the two plasmas on both sides of the DL, the grid boundaries are those of the plasmas. Initially the upstream plasma boundary is left floating (glass plate) and the downstream plasma boundary is a grounded wall (earthed aluminium plate) as in the experiment (figure 4(*g*), section 6). The plasma creation upstream is simulated with an inductive heating process. The loss process imposed in the PIC simulation to mimic the expanding plasma produces an axial decrease in the plasma density and an associated potential drop. The aim of the PIC simulation in this instance is to evaluate if and how the plasma can self-consistently accommodate this phenomenon. It does not say that it will, merely that it can. The imposed decrease of density leads to the formation of a 'narrow' potential drop when the loss frequency is higher than the ionization frequency (figure 10). For a typical density decrease of a factor of 10, the potential drop (which corresponds to a 'forced' Boltzmann expansion) is about 12 V at a pressure of 1 mTorr and for a loss frequency of $10^6\,s^{-1}$. The region defined by the potential drop is about 20 Debye Length, and can be defined as the steady-state double layer of strength 2. The corresponding plasma potential (dashed line), plasma density (solid line) and ion velocity phase space are shown in figure 11. The self-consistent plasma sheaths and DL can clearly be seen in the ion velocity phase space plot as well as the ion beam downstream. The diagnosis of the floating source end wall and the grounded chamber end wall demonstrates that

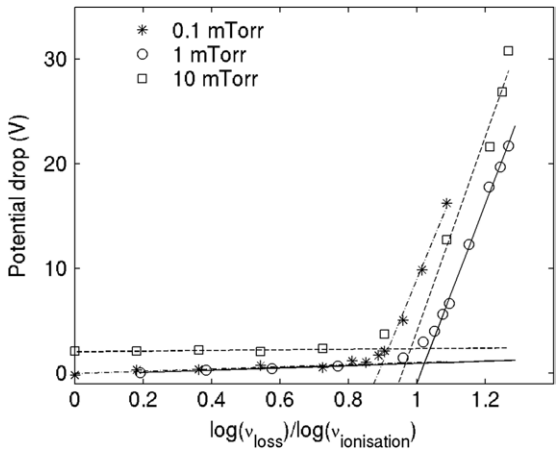

Figure 10. Results from the PIC simulation of CFDL (Meige *et al* 2005a, 2005b): double layer potential drop ϕ_{DL} as a function of the loss frequency.

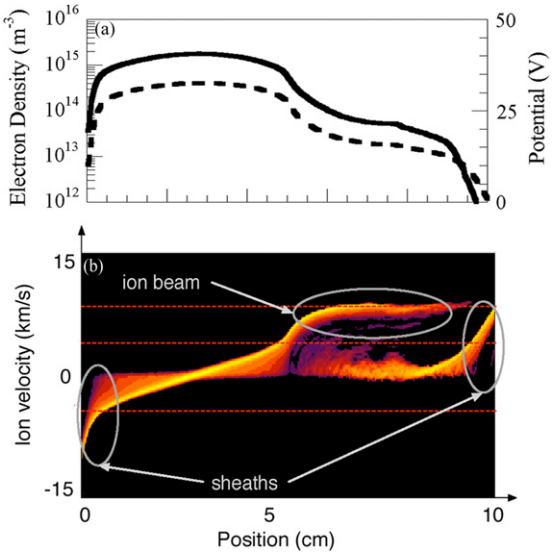

Figure 11. Results from the PIC simulation of CFDL (Meige *et al* 2005a, 2005b, Sun *et al* 2005): (top panel) typical PIC simulated double layer profiles of steady-state plasma density (solid line) and steady-state plasma potential (dashed line) as a function of the axial position; (bottom panel) ion velocity distribution in phase space (increased brightness indicates increased density).

the DL is current-free in this configuration and the DL is maintained when grounding the left plasma wall. The results of the simulation are compared with the experimental results in section 6.6. The PIC simulation shows that moving the right wall away from the DL does not affect its formation or properties and this important result is to be correlated to simulation results on the electron energy distribution function (EEDF): figure 12 shows the EEDF at different axial positions in the plasma. The electron distribution is Maxwellian in parts with an energybreak corresponding to the potential drop of the DL (Meige and Boswell 2006). This prediction has been recently confirmed by the experiment and is detailed in section 6.7.

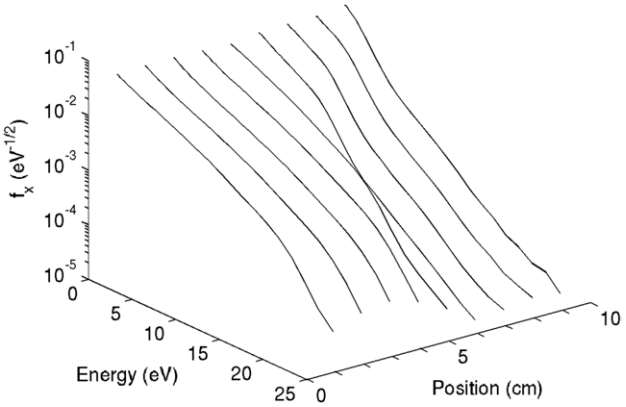

Figure 12. Results from the PIC simulation of CFDL (Meige and Boswell 2006): x-velocity component of the electron velocity distribution function f_x represented in log scale, as a function of the electron energy and at different positions in a double layer plasma. The distributions are Maxwellian for the low energy group of electrons and present a depleted tail at higher energy.

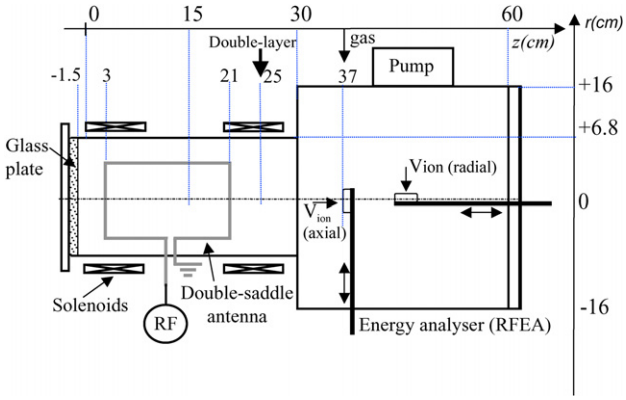

Figure 13. Schematic of one of the CFDL rf expanding devices (figure 4(g)), CHI KUNG, showing major components and probes (Charles and Boswell 2003).

6. Current-free double layers in expanding plasmas

6.1. The rf expanding CFDL device

Recently a new class of CFDLs has been discovered in laboratory plasmas. This stationary DL spontaneously forms in a current-free plasma expansion in a divergent magnetic field for low operating gas pressure (less than 2 mTorr). As a basis for discussion, the description of the properties of this CFDL follows the chronology of the experimental results related to the CHI KUNG device (Charles and Boswell 2003, Charles 2004, Charles and Boswell 2004a, 2004b, Charles 2005a, 2005b, 2005c) and reports on all other findings related to the MNX (Cohen *et al* 2003), HELIX (Sun 2005, Sun *et al* 2005), WOMBAT (Sutherland *et al* 2005), HDLT (Charles *et al* 2007) DL devices as well as other DL devices (Plihon *et al* 2005a, 2005b). For the purpose of this discussion, the device of Plihon *et al* (2005a, 2005b) will be called LPTP device. Two distinct ion populations have also been measured downstream of a small diameter helicon plasma source suggesting the possibility of DL formation (Shamrai *et al* 2006). In the LPTP device, but in the absence of the diverging magnetic field, a DL may form in a very electronegative plasma and its properties differ somewhat from those described in this section (this electronegative DL is reviewed in section 3.2.3 and 4.1.2).

CHI KUNG, LPTP, WOMBAT, HDLT, HELIX and MNX are linear magnetized helicon heated plasma devices (of various sizes) with a Helmholtz-coil pair placed axially around the plasma source which is contiguously attached to an expansion chamber (figure 4(g)). CHI KUNG and LPTP have similar geometries ($14 \times 30\,\mathrm{cm}^2$ and $32 \times 30\,\mathrm{cm}^2$), WOMBAT ($40 \times 20\,\mathrm{cm}^2$ and $150 \times 100\,\mathrm{cm}^2$) and HELIX ($10 \times 61\,\mathrm{cm}^2$ and $200 \times 400\,\mathrm{cm}^2$) are substantially larger devices and all can be set up with a diverging magnetic field. MNX has an additional main chamber ($20 \times 45\,\mathrm{cm}^2$) inserted between the helicon source ($4 \times 30\,\mathrm{cm}^2$) and the expansion chamber ($10 \times 100\,\mathrm{cm}^2$) with the very distinct feature of a magnetic nozzle coil and aperture plate at the junction between the main chamber and the expansion chamber, and a pressure gradient of a factor of 10 between the two chambers. The nozzle coil produces a converging-diverging magnetic field structure (similar to a magnetic Laval nozzle) with a local maximum of up to 2.5 kG. Operation of the helicon source in MNX typically corresponds to the high density blue-core mode with an applied magnetic field of 200–1200 G. All devices present some differences associated with plasma boundaries (floating, conducting, grounded, biased), operating rf frequency (7–30 MHz), location of gas inlet and pumping systems and pumping speeds. In HELIX the source is terminated by a grounded metal wall where currents can close and a differential pumping leads to a pressure gradient of a factor of 10. HDLT is, in essence, a copy of the CHI KUNG plasma source set up as a plasma thruster designed to be immersed in the IRUKANDJI vacuum chamber (section 8.3).

The CHI KUNG experimental device is a horizontal helicon system consisting of a 15 cm diameter helicon source (32 cm long cylindrical glass tube terminated with a 1 cm thick glass plate and surrounded by a 20 cm long double-saddle antenna) attached contiguously to a 30 cm long 32 cm diam earthed aluminium diffusion chamber (figure 13). The source walls are insulating while the chamber walls are grounded. The antenna is fed from a rf matching network/generator system operating at 13.56 MHz. A turbo-molecular/rotary pumping system is connected to the sidewall of the chamber and provides a base pressure of 2×10^{-6} Torr, the pressure being measured with an ion gauge and a baratron gauge, both attached to the diffusion chamber. Argon feed gas is connected to the sidewall of the chamber or to the left end of the source. Two solenoids situated around the source are used to create an expanding magnetic field of 50–250 G in the source centre decreasing to a few tens of Gauss in the diffusion chamber (figure 14). The main external parameters are the gas flow rate and operating gas pressure, the radiofrequency power and the magnetic field configuration. The DL is characterized spatially and temporally. Other effects such as pumping rates and geometry are discussed. In CHI KUNG, the reference parameters correspond to an argon pressure of ~0.2–0.3 mTorr, an rf power of 250 W and a magnetic field of about 130 G in the source region near the DL. Since various plasma source lengths have been used over the years, the z-axis reference is always chosen to be $z = 30$ cm at the junction between the source and the diffusion chamber.

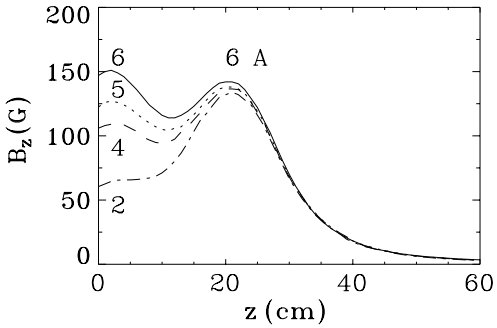

Figure 14. B_z component of the dc magnetic field measured along CHI KUNG z-axis for a constant solenoid current near the source exit (6 A) and a varying solenoid current near the closed end of the source: 6 A (solid line), 5 A (dotted line), 4 A (dashed line) and 2 A (dotted-dashed line); (Charles 2005c).

6.2. Potential and density profiles, DL strength and thickness

Experimental evidence of DL formation in the CHI KUNG device (Charles and Boswell 2003) was initially obtained by using an axially movable retarding field energy analyser (RFEA) oriented to measure ions in the radial direction (aperture hole facing the reactor's walls). In this configuration, the RFEA measures the local plasma potential accurately (Charles *et al* 2000). The results on the plasma potential and density along the z-axis are shown in figure 15 for a pressure of 0.2 mTorr. The total ion flux in the radial direction corresponds to the RFEA measurement for a zero discriminator voltage $I(V_d = 0\,\mathrm{V})$. The Bohm velocity is assumed for the ions and a disc-shaped Langmuir probe is used to calibrate the analyser in density (Charles *et al* 2000). The rapid and discontinuous change in the plasma potential of about 25 V at $z = 25$ cm is that of the DL, ϕ_{DL}, and is accompanied by a discontinuity in the density (figure 15). Downstream of the DL, the plasma can be characterized as 'flowing' and interpretation of the RFEA ion current can be difficult as the flow is supersonic. However, with the RFEA oriented radially, only the thermal ion population $n_i(z)$ is detected and ions accelerated by the DL (n_i is defined in the CFDL model as the thermal ion density $n_a = n_{a1} + n_{a2} \sim n_{a1}$) are excluded. Measurements of the electron temperature using a non-compensated planar Langmuir probe gives an electron temperature of 10 and 8 eV (± 1 eV) upstream and downstream of the DL, respectively, yielding a DL strength $(e\phi_{DL}/kT_{e\ down}) \sim 3$. Recent measurements of EEDFs using a rf compensated Langmuir probe (section 6.9) show that $kT_{e\ down} \sim 5.5$ eV at a pressure of 0.3 mTorr (in excellent agreement with the CFDL model), giving a DL strength of 5. Combining results from HELIX (Sun *et al* 2005, Biloiu *et al* 2005), MNX (Cohen *et al* 2006), the PIC simulation (Meige *et al* 2005a, 2005b), and the CFDL model (Lieberman *et al* 2006), it is found that the strength is in the 2–5 range over most of the operating pressure range, which is less than the potential drop (for these gasses) created by a wall sheath to ensure current equality. Hence, there is a flow of electrons over the DL which can easily neutralize the ion beam created by the DL and may create plasma downstream. At very low pressures (at the limit of the DL pressure range), a strength of 7 and 10 has been reported in WOMBAT (Sutherland *et al* 2005) and in the CFDL model (Lieberman *et al* 2006), respectively. A maximum strength of 7 has also been reported in MNX

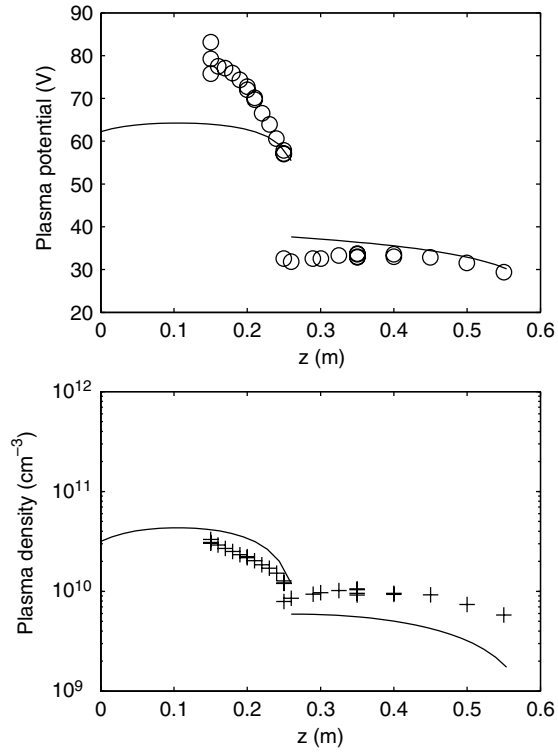

Figure 15. (open circles, top panel) Plasma potential and (crosses, bottom panel) plasma density measured in the CHI KUNG CFDL device (Charles and Boswell 2003) with the energy analyser along the z-axis for 0.2 mTorr pressure, 250 W rf power and high field (figure 14) conditions, respectively; Theoretical results of potential (solid line, top panel) and thermal ion density (solid line, bottom panel) versus position z at 0.2 mTorr (Lieberman and Charles 2006, Lieberman *et al* 2006); to facilitate the visual comparison with the experiment, the theoretical double layer is positioned at $z = 0.25$ m, where measured, rather than at the junction between regions 1 and 2 ($z = 0.30$ m). Hence the actual theoretical data extend to $z = -0.05$ m since the input source length is 30 cm.

with an aperture plate near the centre of the source chamber (Sun *et al* 2005), and a strength of 10 in the same device just downstream of the aperture plate (Cohen *et al* 2006). The DL thickness d is found to be less than 50 Debye lengths in CHI KUNG, WOMBAT (measured with an RFEA) and in the PIC simulation and between 30 and 600 Debye lengths in MNX and HELIX (measured using laser induced fluorescence). In summary the CFDL is classified as weak and magnetic field aligned.

6.3. Ion beam downstream of the DL

6.3.1. RFEA. To get some insight into ion beam formation created by the potential drop ϕ_{DL} of the double layer, the RFEA is subsequently inserted through the diffusion chamber sidewall using the chamber sideport ($z = 37$ cm) closest to the double layer position ($z = 25$ cm). By rotating the RFEA on its support tube axis, measurements are made with the entrance orifice facing the double layer (axial measurement, $a = 0°$) or facing the chamber sidewalls (radial measurements, $a = 90°$). The RFEA can also be moved along the chamber diameter (r-axis on figure 13). The internal radii of the source tube and diffusion chambers are $r = 6.8$ and $r = 16$ cm, respectively.

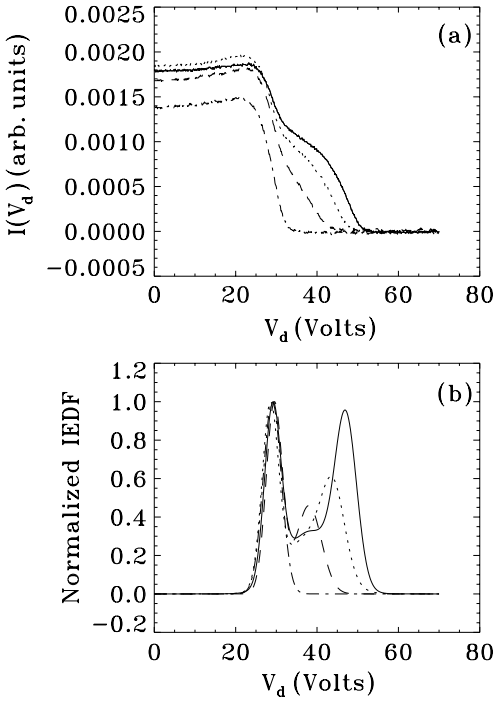

Figure 16. (*a*) $I(V_d)$ characteristics and (*b*) normalized IEDFs obtained in the CHI KUNG device (Charles and Boswell 2004a) with the RFEA located at $z = 37$ cm and $r = 0$ cm for various collection angles: (solid line) $a = 0^0$ (axial measurement with RFEA facing the DL), (dotted-dashed line) $a = 90^\circ$ (radial measurements with RFEA facing the chamber sidewalls), (dotted line) $a = 22^\circ$, and (dashed line) $a = 45^\circ$; operating conditions correspond to a pressure of 0.35 mTorr, a rf power of 250 W and a magnetic field B_z decreasing from about 130 G at $z = 25$ cm to about 50 G at $z = 37$ cm (figure 14).

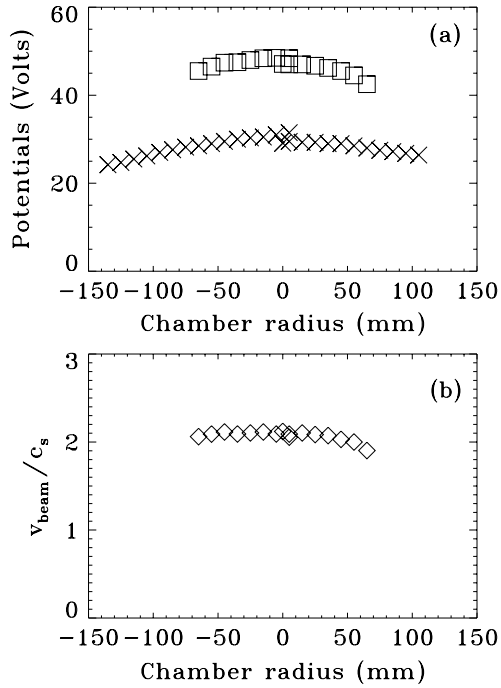

Figure 17. (*a*) V_{beam} (open squares) and V_p (crosses), and (*b*) velocity ratio (open diamonds) calculated using equation (12) across the chamber radius obtained in the CHI KUNG device (Charles and Boswell 2004a) with the RFEA located at $z = 37$ cm and facing the DL ($a = 0^\circ$); same operating conditions as figure 16. The internal tube radius is 6.8 cm.

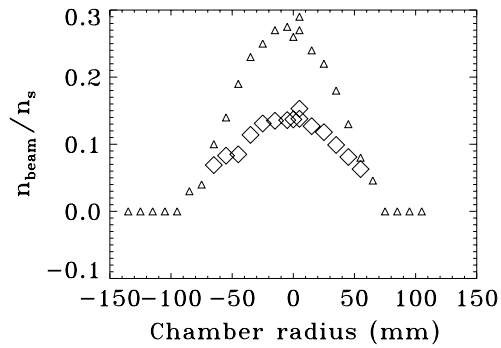

Figure 18. Density ratio (open diamonds) across the chamber radius obtained with the RFEA located at $z = 37$ cm and facing the DL ($a = 0^\circ$). The small open triangles correspond to the upper limit of the density ratio derived from the Gaussian fits (includes all broadening/resolution effects); same operating conditions as figure 16. The internal tube radius is 6.8 cm (Charles and Boswell 2004a).

In this configuration, laboratory evidence of a supersonic ion beam is found for a hydrogen (Charles 2004) and for an argon plasma (Charles and Boswell 2004a). Example of the RFEA $I(V_d)$ characteristic and normalized ion energy distribution function (IEDF) is shown in figure 16 for various rotation angles of the RFEA. The energy gain of $\sim 0.7e\phi_{DL}$ by ions across the DL compares well with the energy gain by electrons ($0.7e\phi_{DL} \leqslant E_{beam} \leqslant 0.9e\phi_{DL}$) measured in current driven DLs (Quon and Wong 1976, Chan *et al* 1984, 1986). The beam average velocity can be written as

$$v_{beam} = \sqrt{\frac{2e(V_{beam} - V_p)}{M}} \sim \sqrt{\frac{4.5kT_e}{M}} \sim 2.1c_s \sim 11\,\mathrm{km\,s^{-1}}, \quad (12)$$

which is supersonic (c_s is the Bohm velocity). The data fit gives the radial profiles of the local plasma potential V_p (crosses), the beam energy V_{beam} (open squares) and of the velocity ratio v_{beam}/c_s, shown in figure 17, respectively. Both V_p and V_{beam} decrease with increasing radius but the ion velocity ratio is constant (∼2) across the source tube suggesting a uniform potential drop ϕ_{DL} across the source. The estimated density ratio n_{beam}/n_s along r is shown by open diamonds in figure 18: it varies from about 6% at the source tube edge to about 15% on the z-axis. This accelerated population is defined as n_{b1} in the CFDL model. Positioning the RFEA on the second side port of CHI KUNG ($z = 50$ cm) shows the effect of elastic and charge exchange ion–neutral collisions (figure 19).

6.3.2. LIF There is a remarkable agreement between the RFEA characterization of the ion beam and the non-perturbative, spatially resolved measurements of ion velocity distributions obtained in argon by laser induced fluorescence (LIF). LIF gives access to parallel and perpendicular flow velocities and ion temperatures and have been carried out in MNX, HELIX and CHI KUNG by using a portable low-power tunable diode laser or a higher power tunable dye laser. The LIF signal versus laser frequency measured just downstream of the DL clearly shows the presence of the slow (trapped ion population, figure 3) and fast (accelerated ions, figure 3) ion groups. A typical spectrum is shown in figure 20. The

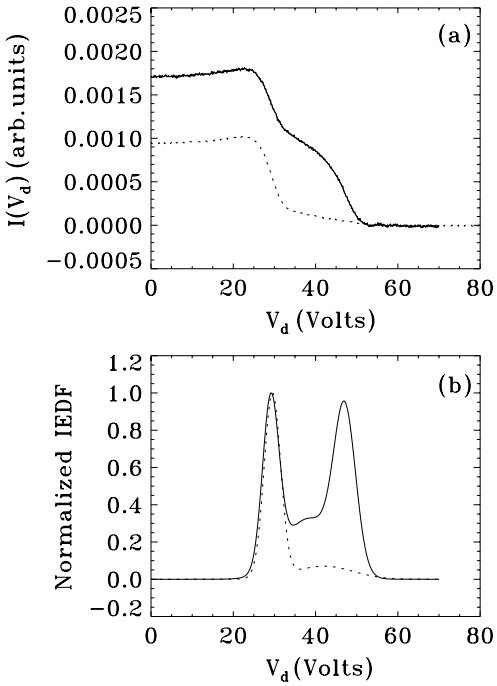

Figure 19. (*a*) Axial ($a = 0°$, facing the DL) $I\,(V_\mathrm{d})$ characteristics and (*b*) normalized IEDFs obtained in the CHI KUNG device (Charles and Boswell 2004a) with the RFEA located at (solid line) $z = 37$ cm and (dotted line) $z = 50$ cm; same operating conditions as figure 16.

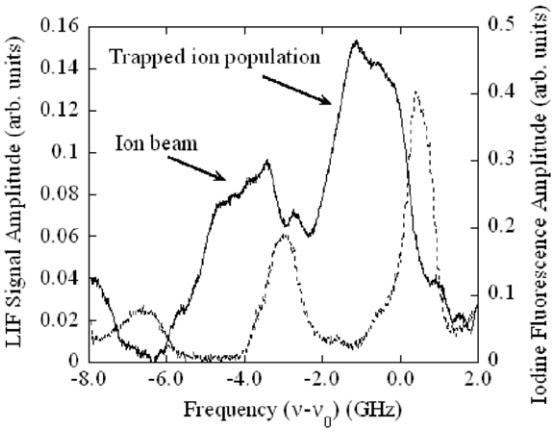

Figure 20. Typical LIF signal versus laser frequency showing the beam and trapped ion populations (solid line) in CHI KUNG (Keese *et al* 2005). Also shown is the iodine cell fluorescence spectrum for the same scan of the laser frequency (dashed line); 0 GHz on the abscissa corresponds to ν_0, the zero-velocity location of the line centre.

values of the parallel ion flow speed are in good agreement with those measured by the RFEA, typically 6–10 km s^{-1} in CHI KUNG (Sun *et al* 2005, Keese *et al* 2005, Keese 2006) and in HELIX (Sun *et al* 2004, Sun 2005, Biloiu *et al* 2005). This non-perturbative diagnostic also leads to accurate measurements of ion temperatures, typically $kT_\mathrm{i} = 0.2$–0.3 eV in the CHI KUNG plasma source in argon (Keese *et al* 2005). Extensive LIF studies have been carried out in the MNX and HELIX devices both in continuous and pulsed modes and the results are discussed in the various subsections below. The ion velocity phase space plots are shown in figure 21.

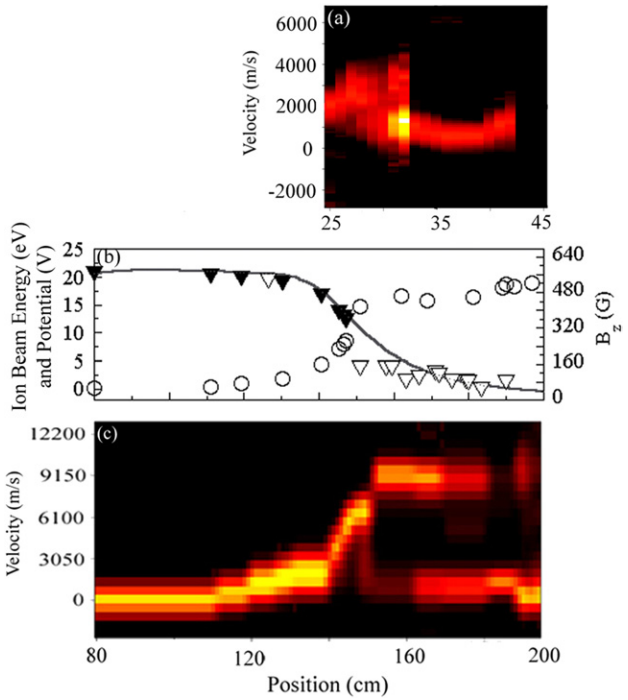

Figure 21. (*a*) Logarithm of amplitude of parallel ion velocity distribution function (colour bar) versus parallel velocity and axial position as measured by LIF in CHI KUNG. (*b*) DL potential difference (plasma potential—9.8 V) versus axial position as measured with a rf compensated, planar Langmuir probe in HELIX (open triangles), ion-beam energy as measured with LIF (open circles), predicted upstream potential difference based on ion beam data (solid triangles) and axial magnetic field strength (solid line). (*c*) Logarithm of amplitude of parallel ivdf (colour bar) versus parallel velocity and axial position in HELIX. Figure components (*a*), (*b*) and (*c*) have been aligned by location of the beginning of rapidly expanding magnetic field (Sun *et al* 2005).

6.4. Time development of the CFDL and source wall charging

The RFEA results on the argon ion beam obtained for continuous excitation (CW) correspond to a time-average measurement which could mask any spatial or temporal stability of the DL. The time development of the argon ion beam is obtained by pulsing the discharge and measuring the total ion current and the ion beam current during the first few milliseconds using the RFEA (Charles and Boswell 2004b) and by comparing these results with a non-DL case corresponding to a lower field configuration (40 G in source centre to a few G in chamber) and higher operating pressure (1.3 mTorr). This non-DL case is similar to previous breakdown studies (Boswell and Vender 1995, Charles and Boswell 1995b, Smith *et al* 1997, Charles and Boswell 1998). A pulse generator controls the rf generator and a 30 dB coupler is used to monitor the forward and reflected powers. The plasma is pulsed with a 2 ms 'on' period and a 10 ms 'off' period, allowing extinction of the plasma between pulses. The tuning is initially set for the CW mode and only slightly adjusted for minimum reflected power at the end of the 2 ms pulse. The rise time of the rf generator measured using the forward power on the coupler is 50 μs and the results are averaged over many pulses. Two Langmuir probes are placed on the z-axis to monitor the time dependence of the floating potential upstream ($z = 7$ cm) and

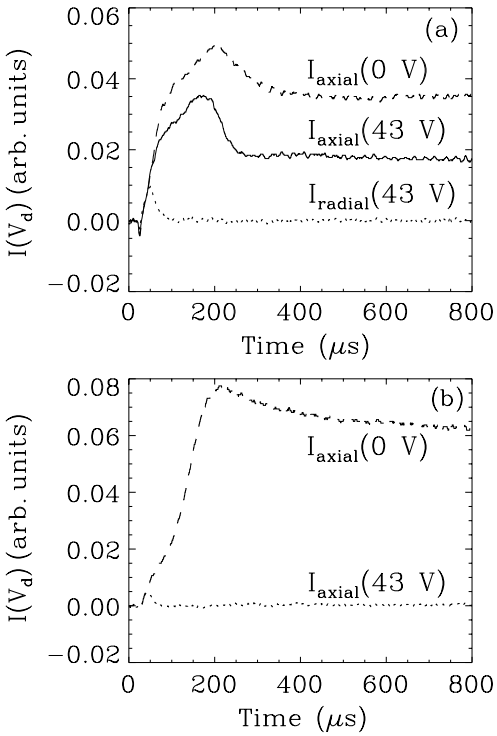

Figure 22. Ion current measurements versus time in the pulse (2 ms 'on'/10 ms 'off') obtained in the CHI KUNG device (Charles and Boswell 2004b) with the RFEA located on axis at $z = 37$ cm for the (a) DL case (pressure of 0.3 mTorr and rf power of 800 W) and (b) 'non-DL' case (pressure of 1.3 mTorr and rf power of 250 W): $I_{axial}(0\,V)$ (dashed line), $I_{axial}(43\,V)$ (solid line) and $I_{radial}(43\,V)$ (dotted Line).

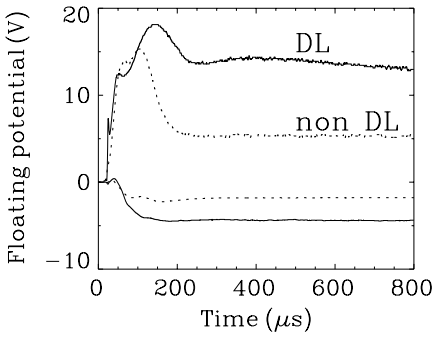

Figure 23. Floating potential versus time in the pulse (2 ms 'on'/10 ms 'off') obtained in the CHI KUNG device (Charles and Boswell 2004b) with the Langmuir probes upstream at $z = 7$ cm (positive curves), and downstream at $z = 57$ cm (negative curves) of the double layer for the DL case (solid lines) and for the 'non-DL' case (dotted lines), respectively. The values measured for the CW mode are 14.3 V, −3.8 V for the DL case and 4 V and −2 V for the 'non-DL' case, respectively.

downstream ($z = 57$ cm) of the DL by a direct connection to a 1 MΩ oscilloscope. Two discriminator voltages on the RFEA are selected, $V_d = 0$ V ($v_0 = 0$) where ions of all energies are collected and $V_d = 43$ V ($v_0 = v_{beam}$) where only ions with energies greater than 43 V are collected: figures 22(a) and (b) show the results obtained for the DL case and for the non-DL case, respectively. The axial measurement of the total ion current $I_{axial}(0\,V)$ (dashed line) shows typical breakdown characteristics.

Evidence of the high energy electrons before the Debye length becomes smaller than the source radius (i.e. before sheaths can exist), followed by the high energy ions streaming out when the plasma potential is large, is clearly shown by the initial small 'negative' and subsequent 'positive' excursions in the measurement of $I_{radial}(43\,V)$ in the pulse (dotted line on figure 22(a)). $I_{radial}(43\,V)$ corresponds to the collection with the RFEA facing the walls of ions with energies greater than 43 V. Following the first electron bump, the second bump in $I_{radial}(43\,V)$ (also seen in $I_{axial}(0\,V)$) corresponds to the high energy ions escaping the plasma in all directions when the plasma potential is very large. Following breakdown, $I_{radial}(43\,V)$ is zero, in agreement with the CW results in figure 16(a) (dotted–dashed line) where no high energy ions are detected when the RFEA is not facing the DL. Looking at $I_{axial}(0\,V)$, for both conditions the ion current (plasma density) increase follows a similar timescale of about 250 μs to achieve equilibrium. However, for the DL case, there is a quite distinct decrease in the ion beam current $I_{axial}(43\,V)$ at 200 μs suggesting that the total ion current measured downstream of the DL is significantly affected by its presence.

Further analysis can be made by using the temporal evolution of the upstream and downstream floating potential as a guide (since a temporal measurement of the plasma potential itself is not an easy task) and the results are shown in figure 23 for the DL case (solid lines) and for the non-DL case (dotted lines). V_f is about 15 V upstream and 5 V downstream. The difference between the two regions separated by the DL is very clear and present: the upstream region has positive floating potentials (15 V) and the downstream region negative floating potentials (−4 V). For the DL case, the floating potential in the source has a temporal evolution similar to that of the total ion current $I_{axial}(0\,V)$ (figure 22(a)). The difference between the DL case and the non-DL case in the source appears to imply wall charging of the source tube and end glass plate (figure 23). Wall charging effects have been often reported in these plasma sources and the high value of the floating potential (∼15 V) in the source seems to be a key indicator for the CFDL formation. Similar results on pulsed DL operation have been obtained in the LPTP device (Plihon *et al* 2007) using an RFEA. In summary, the CFDL is formed in the first 100 μs or so of the discharge well before the plasma has come to equilibrium. The DL is stable thereafter and there has been some evidence using time-resolved LIF of a longer time scale (⩾100 ms) involved in reaching the steady state in HELIX (Biloiu *et al* 2005). The pulsed LIF measurements also show that during the 100 ms long pulse, the fast ion group exhibits a beamlike distribution function of small energy spread about 0.18 eV (consistent with the acceleration in the DL potential drop) while the slow ion group exhibits an increasing energy spread to about 0.5 eV.

6.5. External parameter range of the CFDL: pressure, magnetic field, geometry, rf power

6.5.1. Pressure. A detailed investigation of the parameter ranges leading to the formation of the CFDL has been carried out. The positive floating potential measured upstream of the DL suggests the presence of a large plasma potential in the source (V_{source}). The main parameters V_{source}, V_{beam}, $V_{chamber}$ and ϕ_{DL} are shown as a function of operating gas pressure

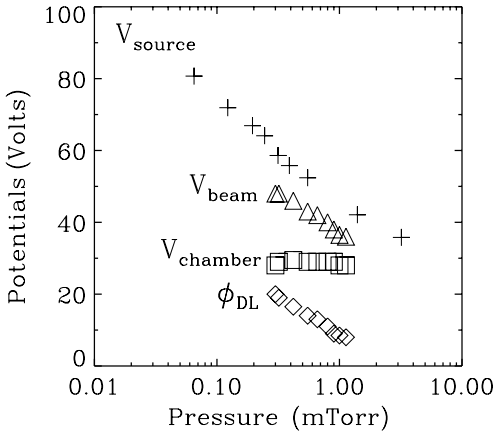

Figure 24. Plasma potential in the source V_{source} (crosses, $z = 15$ cm), ion beam energy V_{beam} (triangles, $z = 37$ cm), plasma potential in the chamber $V_{chamber}$ (squares, $z = 37$ cm) and double layer potential drop ϕ_{DL} (diamonds, $z = 37$ cm) as a function of gas pressure for 250 W rf power and the maximum field condition shown by a solid line on figure 14 (Charles 2005c).

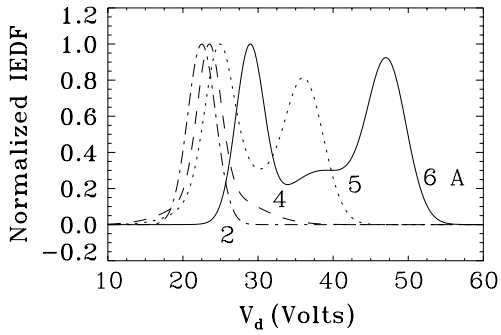

Figure 25. Normalized IEDFs obtained with the RFEA located on axis at $z = 37$ cm and facing the source for the four magnetic field cases shown in figure 14: coil current near the closed end of the source of 6 A (solid line), 5 A (dotted line), 4 A (dashed line) and 2 A (dotted–dashed line). The rf power and gas pressure are 250 W and 0.3 mTorr, respectively (Charles 2005c).

in figure 24 (Charles 2005c). At 0.3 mTorr, V_{source} is 58.6 V, V_{beam} is 48 V, ϕ_{DL} is 20 V. Figure 24 shows that V_{source}, ϕ_{DL} and V_{beam} decrease by the same amount with increasing pressure (while the plasma potential $V_{chamber}$ downstream of the DL remains fairly constant at around 29 V), probably as a result of enhanced collisionality within the plasma which reduces the electron temperature (Lieberman and Lichtenberg 1994). Similar results are obtained in the LPTP source (Plihon *et al* 2007). For pressures above 1 mTorr, the mean free path for ion–neutral collisions (charge exchange and elastic collisions) is a few cm which is a few times less than the distance of 12 cm between the DL and the RFEA and only a tail of hot ions (weakening with increasing pressure) is observed on the IEDF. The DL may still exist and may also shift axially but any beam formed while traversing the DL will have its energy transferred to neutrals over a distance of a few mean free paths (Charles and Boswell 2004a, 2004b). Above a few mTorr, collision processes will lead to an ambipolar diffusion of the plasma from the source to the chamber, well described (Charles and Boswell 2003) by the Boltzmann relation ($n(z) = n_0 \exp(e\phi(z)/kT_e)$). Pumping speeds ranging from 50 to 1200 l s^{-1} have been investigated showing that the gas flow rate has little effect on the formation of the DL for a constant operating pressure. Hence the pressure is a sensitive parameter for the DL formation and this is investigated further in the next section. An increase in plasma potential upstream of the DL and an increase in parallel ion flow velocity downstream of the DL is obtained by LIF in HELIX (Sun *et al* 2004) when the pressure is decreased. However, in the HELIX source, the floating potential is negative, the termination is grounded, and there is a pressure gradient from the source to the expanding chamber.

6.5.2. Magnetic field. For equal currents in the CHI KUNG solenoids, a minimum source field of about 60 G is necessary for the DL to form (Charles 2005c, Sun *et al* 2005, Plihon *et al* 2007). Measurements in the absence of magnetic field in the helicon source show a single peak IEDF at around 46 V and no double layer. For constant gas pressure and rf power, the current in the solenoid at the exit of the source has a strong effect on the plasma density just upstream of the DL, hence of the ion beam density downstream and little effect on amplitude of the DL (the current in the other coil is set at 6 A). The current in the solenoid next to the end glass plate has a strong effect on the wall charging (the current in the other coil is set at 6 A) as shown by figure 25. The DL is generally formed in the region near the maximum gradient of the diverging field. The position of the DL tracks any forced translation of the solenoids (Sutherland *et al* 2005). This has been recently confirmed in the HDLT immersed in the IRUKANDJI space simulation chamber (West *et al* 2007). The effect of the magnetic field structure is quite complex and not fully determined and a change of device geometry leads to some variation in the results as shown by the LIF study in HELIX (Sun *et al* 2004) and in MNX (Cohen *et al* 2006).

6.5.3. Rf power. The DL is formed over a wide range of rf power (tested up to 1800 W in hydrogen and down to 20 W in argon) with no limitation expected. DL formation occurs for CW and pulsed modes. ϕ_{DL} is not greatly affected by the rf power and a linear increase in both the ion beam density and the downstream plasma density is obtained in the inductive mode when increasing the rf power. Typical density ranges upstream of the DL are 10^{10}–10^{11} cm^{-3} in CHI KUNG, LPTP, HDLT, WOMBAT, 10^{11}–10^{12} cm^{-3} in HELIX and over 10^{12} cm^{-3} in MNX.

6.5.4. Geometry. Although the position of the solenoids relative to the tube/antenna geometry is fixed in the original CHI KUNG experimental design, it is possible to carry out an experiment by adding a second glass plate and shortening the source length. The results in figure 26 show that a beam density increase by a factor of three can be obtained with the second glass plate positioned at the maximum of the magnetic field ($z = 2$ cm). This increase in the beam density could result from an increased plasma density upstream of the DL or from a change in the axial position of the DL since the potential drop remains fairly constant. More complex geometries with aperture plates have been investigated by LIF in the MNX devices (Sun *et al* 2005, Cohen *et al* 2006). In summary, the configuration of the divergent magnetic field, the operating

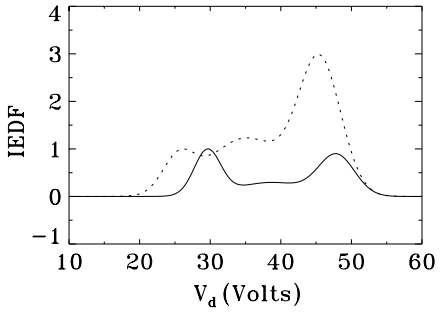

Figure 26. IEDFs obtained with the RFEA located on axis at $z = 37$ cm and facing the source without (solid line) and with (dotted line) the addition of a second glass plate at $z = 2$ cm. For better clarity, the IEDF is normalized using the low energy peak corresponding to the downstream plasma potential. The rf power and gas pressure are 250 W and 0.3 mTorr, respectively and the maximum field condition shown by a solid line on figure 14 is used (Charles 2005c).

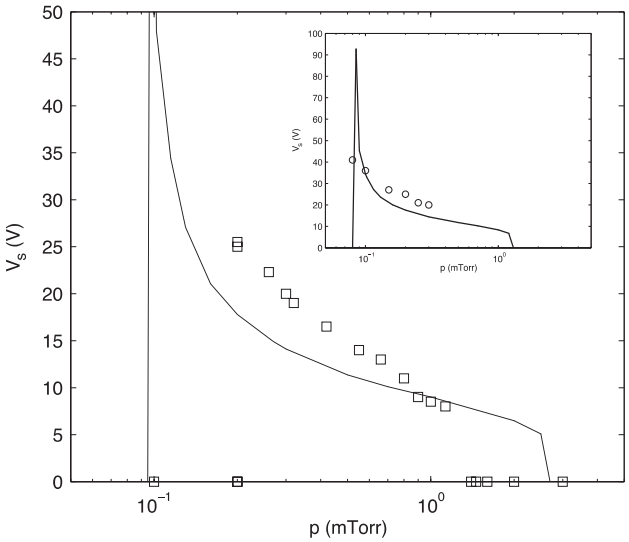

Figure 27. Pressure variation of the double layer strength V_s (Lieberman *et al* 2006): theoretical (solid line) and experimental (open squares) results in CHI KUNG; inset is for a larger device (Sutherland *et al* 2005): measurements (open circles) and theory (solid line).

gas pressure and the source geometry are important external parameters affecting the DL formation and its characteristics.

6.6. Comparison with the PIC simulation

The loss process imposed in the PIC simulation (Meige *et al* 2005a, 2005b) to mimic the expanding plasma produces an axial decrease in the plasma density and an associated potential drop and a direct comparison between the measured and simulated density on axis is not valid for a weak DL. The simulated DL thickness is about 20 Debye Length, and its strength is about 2. The simulated ϕ_{DL} is lower than that measured experimentally and does not vary much with gas pressure. However, all other information on particle distributions, DL boundary conditions and plasma boundary conditions is of primary importance. The diagnosis of the floating source end wall and the grounded chamber end wall demonstrates that the DL is current-free and stable. The floating source end charges to about 10 V in good agreement with the experiment. Simulated results on the ion beam formation and its observation downstream agree very well with the experiments (RFEA and LIF) as shown by figure 11 (bottom panel) and figure 21 (bottom panel). In the simulation, the upstream ions enter the DL with the Bohm velocity. The simulated EEDF clearly shows the two-electron populations upstream (trapped and passing) and the comparison with the experiment is reported in the 'electron dynamics' (section 6.9).

6.7. Comparison with the CFDL model

The pressure variation of the double layer strength V_s in argon obtained from the theory and the experiment with the RFEA is shown in figure 27 for CHI KUNG ($h = 31$ cm, $R_2 = 6.85$ cm, $w = 29.4$ cm and $R_1 = 15.9$ cm) and for a larger device (WOMBAT: $h = 57.8$ cm, $R_2 = 10$ cm, $w = 200$ cm and $R_1 = 50$ cm). V_s rises dramatically as the pressure is decreased, with a minimum pressure of approximately 0.1 mTorr for a solution to exist in CHI KUNG. Below that pressure, the maximum (with respect to V_s) ionization rate coefficient for the accelerated electrons upstream is not sufficient to balance the excess upstream particle losses. The maximum double layer strength can be as high as ∼100 V near the minimum pressure, but is a very sensitive function of pressure for such high values of V_s. Both the experiment and the theory show that the plasma is maintained below 0.2 mTorr but the transition is marked by a strong decrease in density by a factor of at least 4, so that the upstream density becomes much lower than the downstream density. Both the theory and the experiment show that the double layer disappears at pressures above about 2 mTorr. The theoretical results of potential V and thermal ion density versus position z at 0.2 mTorr are shown in figure 15. To facilitate the visual comparison with the experiment, the theoretical double layer is positioned at $z = 0.25$ m, where measured, rather than at the junction between regions 1 and 2 ($z = 0.30$ m). The general shape of the potential and the thermal ion density is quite similar to that seen experimentally, but with a somewhat smaller double layer potential V_s. For a gas pressure of 0.2 mTorr, the wall potential is 12 V, the plasma potential upstream of the DL is 60 V, the DL potential drop is 17 V, the left wall sheath potential is about 40 V, the right wall potential is 30 V. An unexplained feature of the experimental results, not seen in the theory, is the large potential rise upstream of the double layer, which may be an artefact of the experimental measurement for z less than 0.2 m, where a non-negligible earthed area (probe shaft) is introduced into the insulated region 2. Other measurements show a plasma potential of about 60 V at $z = 15$ cm with the RFEA and of about 60 V at $z = 17$ cm with a compensated Langmuir probe. The electron temperature obtained with the theory in the downstream region is 5.7 eV, in excellent agreement with recent results obtained with a compensated probe (section 6.9). The plotted density corresponds to the thermal ion density measured using the RFEA when the orifice was oriented at right angles to the exiting ion beam (as in section 7.2). The up ($z = h/2$) to down ($z = h + w/2$) density ratio is about 7. The effect of ion–neutral collisions has been investigated: the theoretical and experimental results for the decay of the relative ion beam density versus position

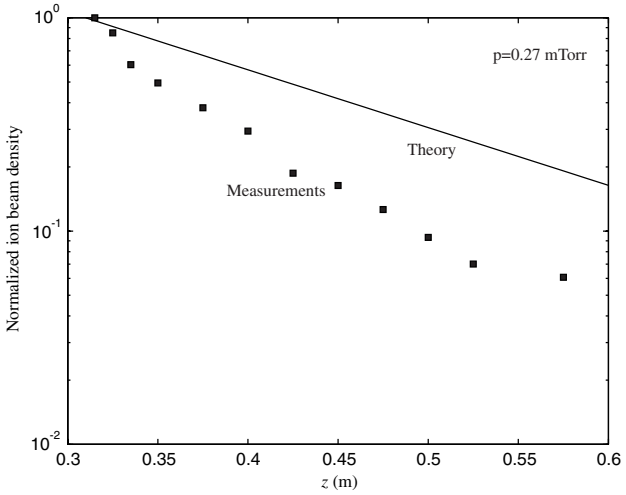

Figure 28. Relative ion beam density versus position z in CHI KUNG, measurements in argon (solid squares); theory for argon (solid line); (Lieberman *et al* 2006).

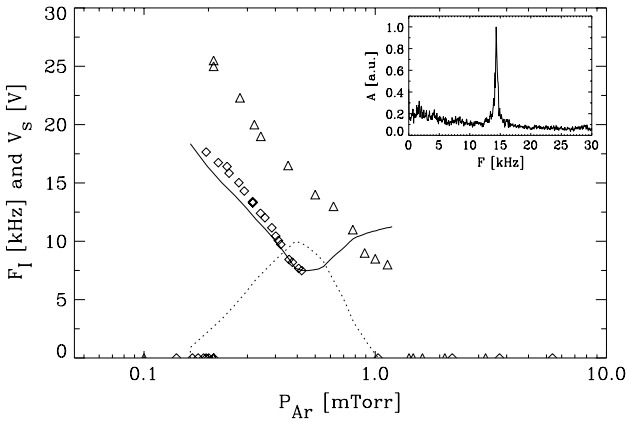

Figure 29. Frequency of instability (diamonds) and potential drop of the double layer (triangles) as a function of pressure in CHI KUNG. Inset is a normalized spectrum at 0.3 mTorr; the solid line shows the theoretical calculation of frequency for a wave number $k_0 = 26\,\mathrm{m}^{-1}$, and the dotted line is the corresponding growth rate (Aanesland *et al* 2006a, 2006b).

are shown in figure 28 at 0.27 mTorr argon. The measured beam decay is somewhat faster than the theoretical decay, but the results are quite sensitive to the uncertainty in the pressure measurement and to the value $\lambda_b \sim 0.7\,\lambda_i$ used in the theory (λ_i and λ_b are the mean free paths in argon for thermal and fast ions, respectively). Similar results on the effect of ion–neutral collisions downstream of the DL have been obtained by LIF in HELIX (Sun *et al* 2004, Biloiu *et al* 2005) and with the RFEA in the LPTP device. The RFEA results have been modelled using ion beam flux conservation downstream of the DL for flat DL and spherical DL profiles (Plihon *et al* 2007).

6.8. Instabilities associated with the CFDL

The RFEA and Langmuir probe as well as an emissive probe have been used to study instabilities associated with the CFDL (Aanesland *et al* 2006a, 2006b). The frequency spectrum of the plasma parameters (floating and plasma potential, ion and electron saturation current) fluctuations is measured over a 1–30 MHz frequency range. The main parameters investigated are the axial position and the operating gas pressure. A low frequency instability in the 5–20 MHz range associated with the presence of the CFDL is measured and interpreted as an upstream ionization instability resulting from the additional ionization caused by the accelerated electrons arriving from downstream. A theory based on the model described in section 4.4 is developed and both the theory and the experiment show that the frequency of the instability increases linearly with the potential drop of the DL as shown in figure 29. It is assumed that the perturbed quantities vary as $\exp(\mathrm{j}\omega t - \mathrm{j}kz)$. These quantities are expressed as a function of the perturbed potential. The perturbed ion balance/continuity relation is expressed solely using the perturbed potential $\tilde{\varphi}$ and rewritten in the form of a Helmholtz equation to solve for the wave dispersion. The wave frequency is obtained for any given wave number k. Using $k = 26\,\mathrm{m}^{-1}$ and a calculated accelerated electrons/total electron density ratio of 0.27, the wave frequency and growth rate are determined versus the gas pressure. The growth rate in the DL pressure range is very small, although positive, in agreement with the small amplitudes seen experimentally.

6.9. Electron dynamics

A cylindrical, rf compensated Langmuir probe has been used to measure the electron energy distribution function (EEDF). The design of the probe (Sudit and Chen 1994) corresponds to an exposed nickel wire 3 mm long and 0.25 mm in diameter connected through a glass to metal seal to five rf choke coils mounted in series to filter any plasma potential oscillation at the fundamental (13.56 MHz) or second harmonic (27.12 MHz) frequencies. The second derivative of the current voltage trace contains the EEDF and the local plasma potential (V_p), the latter being taken as the zero crossing of the curve and the EEDF being the section of the curve to the left of V_p. The second derivative is obtained using a differentiator. Electrons in the plasma see the local plasma potential as a zero reference for the EEDF and the sweeping voltage of the probe uncovers more and more of the EEDF as it approaches V_p from below. Hence the zero reference of the local EEDF actually represents the local V_p. The results are shown in figure 30 for a pressure of 0.3 mTorr, and the standard rf power and field configuration (Takahashi *et al* 2007). In the high potential plasma, upstream of the double layer, the measured EEDF shows a very clear change in slope (ε_{break}) at energies corresponding to the double layer potential drop. Electrons with lower energy are Maxwellian with a temperature of 8 eV whereas those with higher energy have a temperature of 5 eV. The EEDF in the downstream plasma has a temperature of 5 eV. Over the range of pressures where the double layer and accelerated ion beam is detected by analysis of a retarding field energy analyser, the strength of the double layer corresponds to the ε_{break} in the EEDF as predicted by the PIC simulation (Meige and Boswell 2006). It is deduced that the downstream electrons come from upstream electrons that have sufficient energy to overcome the potential of the double layer, and that only a single upstream plasma source is required to maintain this phenomenon.

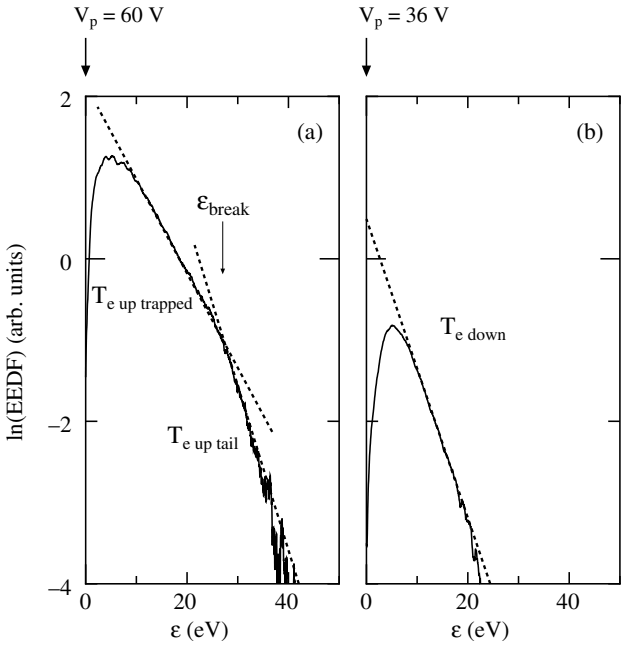

Figure 30. Natural logarithm plot of electron energy distribution functions (EEDF) in (*a*) the upstream area ($z = 17$ cm) and (*b*) the downstream area ($z = 36$ cm) for a pressure of 0.3 mTorr in CHI KUNG. The dashed lines show the tangential lines giving each temperature $T_{e\ up\ trapped}$ (8 eV), $T_{e\ up\ tail}$ (5 eV) and $T_{e\ down}$ (5 eV). The break energy of the EEDF depletion at 27 eV is defined as ε_{break} (Takahashi *et al* 2007).

In the model for the DL (Lieberman and Charles 2006, Lieberman *et al* 2006), a constant electron temperature is assumed over the whole volume, and to explain the increased ionization in the upstream area (a result of the magnetic field configuration) the existence of an electron group accelerated by the DL arriving from the electrons created in the downstream area is assumed: in Andrews and Allen's (1971) model, the electrons entering the DL from the downstream side are assumed mono-energetic while in Lieberman and Charles's (2006) model, a near-half Maxwellian is assumed to calculate the ionization rate coefficient for this electron group. The large ionization from this high energy group of electrons emerging into the upstream plasma with drift speeds several times over the local electron thermal velocity upstream, has been previously derived by Conde *et al* (2001). These three analytical descriptions of the high energy electron group upstream lead to a positive slope in the upstream EEDF. This is verified experimentally in an anode DL device (Conde and Leon 1994): the high energy electrons are observed in the form of a beam in the EEDF measured using a cylindrical Langmuir probe and the beam thermalizes over a short distance (a few cm). In the CFDL device (Takahashi *et al* 2007), the results from a rf compensated cylindrical Langmuir probe have a Druyvesteyn form without any part resembling a Maxwellian in a region extending over a few cm on either side of the DL ($22\,\text{cm} \leqslant z \leqslant 27\,\text{cm}$). In this very inhomogeneous region, it is possible that the Druyvesteyn method or even the probe geometry might be inappropriate (Anderson 1977). However, outside this region, i.e. a few cm upstream from the DL, the results from the rf compensated probe do not show a beam of electrons arriving from the downstream plasma, in the sense that there is nowhere a positive slope in the EEDF (figure 30). It does show that upstream, the depleted tail electrons clearly arrive from downstream and so, on their own, can be considered an accelerated group of downstream electrons entering the upstream population. In this sense, the experimental results are in excellent agreement with the kinetic PIC simulations (Meige and Boswell 2006) which show EEDFs having precisely the same form. The fluid model (Lieberman and Charles 2006) also requires an accelerated group of 'beam' electrons arriving from downstream to satisfy the charge conditions for the existence of the double layer but uses a fluid definition of equal electron temperature both upstream and downstream. Hence, the experimental results, while not showing a classical 'beam' of electrons, do show elements that agree with both the simulation and the fluid model and strongly suggest that both are presently too simplistic to adequately model the details of the experiment. On the other hand, it should be mentioned that the fluid model shows quantitative agreement with the experiment over a wide parameter range and so is able to usefully predict the behaviour of the double layer. However, the details of the kinetic behaviour need to be incorporated in the theory.

In the main chamber of the MNX device, i.e. upstream of the DL, measurements of the EEDF with a non-compensated Langmuir paddle probe combined with optical measurements show the presence (with and without a 2 kG nozzle field) of a small (0.1%) superthermal electron population with an average energy of 10 T_e for a magnetic field of about 700 G and a rf power of 900 W. In comparison with the CHI KUNG EEDF in figure 30, the MNX EEDF exhibits a first linear decrease ($T_e \sim 7$ eV) to an energy of 10 eV followed by a linear decrease of reduced slope ($T_e \sim 25$ eV) up to energies about 60 eV. The corresponding plasma is that of a blue-core helicon mode.

6.10. Global effect

The diagnosis of the various CFDL devices has led to a very good agreement in terms of parameter ranges leading to the formation of the DL, characterization of the slow and fast ion populations, characterization of the bulk electrons with some differences associated with very energetic electrons especially upstream of the DL. Analysis of the presheath acceleration just upstream of the DL has shown measured ion velocities ranging from 1 to 2 times the Bohm velocity using LIF and the RFEA (c_s in the PIC simulation, 1.3 c_s in the theory).

In the present system, energy generated by an external source is fed into the plasma and is absorbed by the plasma electrons. No current or potential is presently imposed as a starting condition but specific boundaries, geometric and magnetic structures are present. The magnetic field configuration is forcing the plasma to expand from the source (insulating walls) to the diffusion chamber (conducting walls). Currents cannot flow from the source to other parts of the reactor. At very low pressures, the collisions are limited, and the plasma forms a double layer near the exit of the source. The experiment, the simulation and the theory show some charging of the source end wall and the DL potential drop is smaller than the left wall sheath potential. The results show that the upstream plasma fully supports the double layer and the downstream plasma rather than the double layer being the interface between two separate and distinct plasmas.

7. Recent development of astrophysics double layers

7.1. Neutron stars

Although the following work has already been reviewed by Raadu (1989), it is of interest to the present report on current-free double layers. In 1986, Williams *et al* (1986), introduced the formation of a strong (relativistic) current-free double layer as an alternative decelerating mechanism for protons in the accretion column of a neutron star in a binary system, especially for low luminosity cases ($\ln 10^{37}$ erg s^{-1}) where radiation pressure is low and the strong magnetic field may damp out the instabilities needed to maintain a collisionless shock. The role of the DL is to transfer ion beam energy ($\sim$100 MeV) to electrons by decelerating the incoming high velocity ion beam (called the 'passing' accreting H^+ population) and accelerating electrons so as to form a downwardly directed relativistic beam (called the 'passing' accreting e^- population). These electrons will radiate their energy in the form of x-rays and gamma rays. These 'passing' accreting populations are added to the passing atmospheric H^+ and e^- populations, and to the trapped H^+ and e^- populations to establish a model where six particle distributions of four types are defined: full Maxwellian for trapped H^+, half Maxwellian for atmospheric H^+ and e^-, waterbag for accreting e^- and a combination of Maxwellian and waterbag for accreting H^+. The high potential region is the star's atmosphere. The model is used to calculate the required distribution of trapped atmospheric electrons which would be consistent with a 'standard' DL potential profile (equation (7)). The DL has no net current and the results are physically reasonable.

7.2. Solar flares, solar corona, solar wind

Models of solar flares including the creation of a DL as a mechanism for releasing the energy stored in a current loop in the solar corona have been proposed from the late 1960s (Raadu 1989). All models of particle acceleration by a coronal DL assume that a current is creating the DL. In the context of solar wind acceleration, large flow velocities (up to 200 km s^{-1}) have been reported at the foot of solar macrospicules (Pike and Harrison 1997). Recently strong observational evidence has shown that the solar wind might originate from coronal funnels (Tu *et al* 2005) and numerical evidence supports that high outflow speeds associated with funnels can cause Ly-alpha intensities consistent with what has been measured (Esser *et al* 2005). Recently it has been proposed (Boswell *et al* 2006) that current-free double layers could be the source of plasma acceleration in solar funnels, pointing out the striking resemblance in plasma parameters between solar funnels and the laboratory CFDL described in section 6: although the physical dimensions of the 'device' are dramatically different (7 orders of magnitude), the plasma density, electron temperature and magnetic field expansion are very similar. The plasma density decreases proportionally to the magnetic field for both systems. The laboratory CFDL has a typical strength of 3 which corresponds to a hundredth of the total energy required to generate the solar wind. Hence it can only provide the initial plasma heating and acceleration in the transition region. It cannot accelerate the solar wind to its terminal speed. While electrons are heated by the rf signal power the DL in the laboratory, an energization of the electrons at the bottom of the funnel still has to be identified. The origin of the electron current is not clear but could be associated with a wave bringing energy from elsewhere (Goertz and Boswell 1979).

7.3. The far side of the Moon

In 2002, Borisov and Mall predicted the existence of a strong DL behind the Moon (Borisov and Mall 2002) based on the formation of an electric potential on the surface of a large non-magnetized moving cosmic body (the Moon) in a plasma (the solar wind). This theoretical analysis was motivated by earlier observations from the Apollo 15 subsatellite (Anderson *et al* 1972) and more recent measurements of potential in the lunar wake obtained on the Wind spacecraft (Ogilvie *et al* 1996) and of electron fluxes by Lunar Prospector (Lin *et al* 1998). It anticipates additional information from the 2005–2006 SMART 1 electric propulsion mission to the Moon (Borisov and Mall 2002, Halekas *et al* 2003). Previous experimental and theoretical studies dealt with weak potentials (a few volts) on the sunlit hemisphere of the Moon. The proposed theory calculates the electric potential build-up on the far side of the Moon which results from the low conductivity of the Moon near its surface and the very different thermal speeds of the electrons and ions in the solar wind. The assumed velocity distribution functions of the electrons and protons both include a Maxwellian core and a non-Maxwellian halo (high energy tail) and absorption of all charged particles reaching the surface of the Moon is assumed. Poisson's equation is solved to find the electric potential and the DL thickness is calculated by finding the potential value where quasi-neutrality holds and the distance where quasi-neutrality breaks down. The higher the speed of the solar wind, the broader and the stronger the DL is. The magnetic field is initially assumed to be orthogonal to the direction of the solar wind. For a moderate solar wind speed of about 400 km s^{-1} the thickness of the DL is about 200 km and its strength about 40. The Moon's conductivity strongly affects the ratio V_m/V_r between the Moon's surface potential at its far side and the potential at the rear boundary of the DL. For example zero conductivity gives a ratio larger than 1 and a conductivity of 10^{-9} S m^{-1} gives a ratio smaller than 1. The theory is used to estimate electron fluxes near the far side of the Moon and these are successfully compared with the available experimental data (Lin *et al* 1998, Anderson *et al* 1972). Since all parameters change over time, the numbers chosen above for the purpose of this review are simply an illustration of the far more complex spatial and temporal system associated with the possibility of a strong DL behind the Moon (Borisov and Mall 2002, Halekas *et al* 2003).

7.4. The Auroral cavity

Analysis and modelling of data from the FAST satellite has led to significant development of the physics of the aurora over the past few years (Newman *et al* 2001, Ergun *et al* 2001, 2002, Andersson *et al* 2002, Main *et al* 2006). The auroral cavity encapsulated at the magnetosphere-ionosphere boundary shows two transition layers with measured parallel electric fields: a high altitude transition layer ($\geqslant$10.000 km from the surface of the Earth) which separates the auroral

cavity from the magnetosphere and a low altitude transition layer (<10.000 km) which separates the auroral cavity from the conducting ionosphere. Measurement and model have shown strong ion acceleration of anti-earthward ion beams, low frequency turbulence and whistler waves in the upward-current region at high altitudes. Similarly, strong electron acceleration of electron phase space holes, lower hybrid waves and dc turbulence occur in the downward-current region at low altitudes. Ion holes and ion cyclotron waves are observed and modelled in the region of mid-cavity DLs. This Alfven dominated region has some similar features to those of the upward and downward current region.

8. Recent applications of double layers

8.1. Dusty plasmas

The importance of the diagnostic and understanding of dusty plasmas has been widely reported both in the field of plasma processing and in connection with matter in the universe in the form of dust grains in an ionized gas (Barkan and Merlino 1995). Dust particles injected in a typical laboratory plasma charge negatively and the electric field of the sheath at the plasma boundary is sufficient to balance the gravity force and electrostatically trap the dust particles. Similarly any high potential region in a plasma may act as an electrostatic trap, and in particular the high potential side of a DL. Barkan and Merlino (Barkan and Merlino 1995) have reported a basic study on the confinement of dust particles (hydrated aluminium silicate) in a nitrogen anode double layer (anode biased at 200 V) near the end of a magnetized (3–4 kG) plasma column (electrons and K^+ ions formed by surface ionization on a 2500 K tantalum plate) in a Q machine. Details on the possibility of grains forming a Coulomb solid and on the effects of plasma rotation and instabilities are discussed.

8.2. Plasma processing

Over the past decade, there has been an increasing use of low pressure high density reactive and non-reactive plasmas for microelectronics and optoelectronics applications. The density and directed energy of the ions impinging onto the surface during processing (etching, sputtering, deposition, surface treatment) are important parameters which result from the plasma source parameters and from the local parameter such as an applied bias to the substrate. Applications which require soft (low energy or flux) surface treatment are numerous (treatment of organic cells or tissues for biological applications, treatment of soft polymer-based planar optical waveguides, treatment of proton exchange membrane in hydrogen fuel cells, etc). Results on the surface functionalization of various films (chalcogenide glass, nafion membrane) using the large area 10–50 eV ion beam produced by the CFDL described in section 6 have been reported (Charles 2006). The low energy treatment of nafion membranes using a CFDL containing plasma has been carried out and a decrease of water contact angle (hydrophobicity) has been correlated with an increase in the ion energy dose (Charles *et al* 2007). This research takes place in the context of the complete fabrication of low temperature hydrogen fuel cells using plasma processes as a replacement for chemical processes, in an attempt to reduce catalyst usage and increase the catalytic activity and the fuel cell efficiency (Brault *et al* 2004, 2006, Ramdutt *et al* 2007, Caillard *et al* 2007).

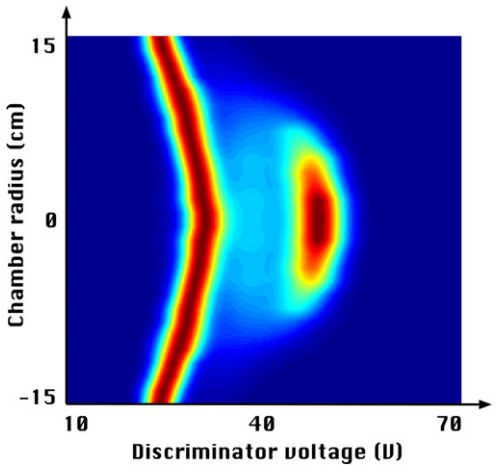

Figure 31. Normalized IEDFs obtained with the RFEA along the chamber diameter in CHI KUNG showing the beam (high energy band) and trapped (low energy band) ion populations. The ion beam is used as a source of thrust in the helicon double layer thruster (Charles 2005a).

8.3. Plasma thrusters

Manheimer (2001) has discussed the application of plasma acceleration by area expansion to space plasma propulsion: a basic theory of the quasi-neutral ECR (electron cyclotron resonance) plasma nozzle leads to estimates of the acceleration. Potential advantages of the 'plasma nozzle thruster' are listed: absence of electrodes, no need for a neutralizer, high thrust, high specific impulse and high efficiency. Momentum impartment in a plasma expanding in a diverging magnetic field has been treated theoretically (Fruchtman 2006) and has shown that the increase of plasma thrust may result from magnetic field pressure in a situation where there is no potential difference between the plasma edges. Magnetic plasma expansion designed to accelerate the plasma and convert the perpendicular ion energy into parallel ion energy is used in the thruster experiment Variable Specific Impulse Magnetoplasma Rocket (VASMIR) plasma rocket (Chang-Diaz 2000). In general, capacitive, inductive or Helicon rf sources are of interest to the field of electric propulsion (Cohen *et al* 2003, 2006, Beal *et al* 2006, Pucci *et al* 2006, Walker *et al* 2006a, 2006b, Shamrai *et al* 2006, Toki *et al* 2006). Applying a capacitive rf discharge in a dielectric capillary for generating quasi-neutral plasma flow of a few tens of eV can be used as a miniature plasma thruster (Dunaevsky *et al* 2006).

Measurements of energetic ions have been reported since the early 1990s in the expanding region just downstream of ECR (Gottscho *et al* 1991) and helicon sources (Charles 1990, 1993, Charles *et al* 1991, 1992). The CFDL detailed in section 6 is the basis of a new candidate for electric propulsion in space, the helicon double layer thruster, in which the large area supersonic ion beam generated near the exit of the plasma source is the source of thrust (Charles and Boswell 2002, 2003, Charles 2004, Charles and Boswell 2004, Charles 2005a, 2005b, 2005c) as shown by figure 31. The HDLT

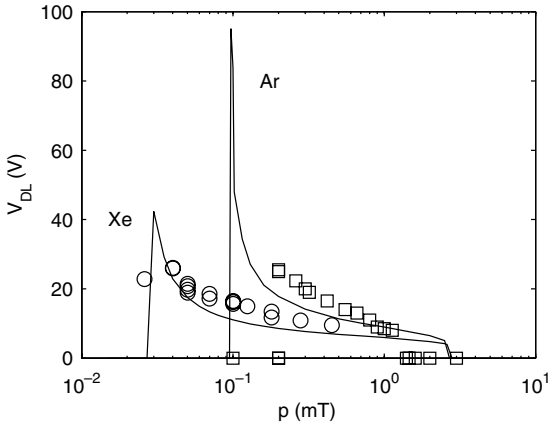

Figure 32. Double layer strength V_{DL} versus pressure in CHI KUNG: theoretical (solid line) and experimental (open circles) results for xenon (Charles *et al* 2006b).

is simple, safe, has no moving parts, no electrodes, and no need for an external neutralizer. Hence it can be defined as a new type of magnetoplasma thruster with anticipated long life characteristics most adapted to interplanetary travel or large Earth orbit manoeuvres. It can operate with a variety of propellants (argon, hydrogen, xenon, oxygen), both in pulsed and in continuous modes and can be scaled up or down both in terms of size and power. The first prototype was built and tested in 2005 in a 4 m long, 2 m in diameter space simulation chamber at the European Space Agency test centre in The Netherlands. Although DL diagnostics and thrust measurements were not available during the short course of the testing campaign, successful ignition and steady-state operation of the HDLT was achieved for a large range of rf power, xenon gas flow rates, and magnetic field strength (Charles 2005a, 2005b, Charles *et al* 2006a). Tests of the HDLT prototype mounted on a standard laboratory chamber have shown that a CFDL can be generated in xenon, the inertial gas used in electric propulsion due to its large ion mass, and the behaviour of the DL with pressure has been successfully modelled using the theory described in section 4 (Charles *et al* 2006b). The results are shown in figure 32. The formation of the CFDL has been recently measured using an RFEA with the HDLT prototype immersed in the smaller IRUKANDJI vacuum chamber (West *et al* 2007). A simulation study of plasma detachment in the exhaust of the HDLT has shown that for standard operating conditions, the plasma beam detachment occurs about 10 cm downstream of the thruster cavity (Gesto 2005, Gesto *et al* 2006). Plasma detachment in/from a magnetic expansion, e.g. in plasma-based space propulsion systems (Hooper 1993, Arefiev and Breizman 2005) or in the solar wind (Parker 1958) is a problem that is still under active research and has been known to produce spirited debates.

9. Conclusion

The recent developments in laboratory double layer experiments have been reviewed. The past two decades have been marked by the technological development of low pressure, high density rf inductive/wave plasma sources for the microelectronics industry, the associated increase in computer power at low cost and the unprecedented acquisition of high spatial and temporal resolution of satellite data. In addition to the further development of the original mostly current-driven DL devices (discharge tubes, double and triple plasma devices, single and double-ended Q machines), two new types of mostly current-free DLs have been discovered in expanding plasmas: the first in the expansion of a pulsed two-electron-population expanding plasma at very low pressure (no stationary ions downstream) and the second in a current-free rf expanding inductively coupled plasma. These weak current-free DLs share many aspects with weak current-driven DLs and possibly with the strong DLs observed in the auroral cavity. Computer simulations and analytical modelling of both the laboratory and the astrophysics DLs have been developed and some of the results are in good agreement with the experimental data. However, many fundamental aspects remain unclear. Recently, application of double layers to the field of plasma thruster has attracted much interest and its development may shed some light into fundamental problems in astrophysics such as plasma detachment from a magnetic field.

Acknowledgment

Many thanks to the Tomaga River Mouth for providing beautiful waves during the endless summer of 2007.

References

Aanesland A and Charles C 2006 *Phys. Scr.* T **122** 19
Aanesland A, Charles C, Lieberman M A and Boswell R W 2006a *Phys. Rev. Lett.* **97** 075003
Aanesland A, Lieberman M A, Charles C and Boswell R W 2006b *Phys. Plasmas* **13** 122101
Aflori M, Amarandi G, Ivan L M, Dimitriu D G and Sanduloviciu M 2005 *IEEE Trans. Plasma Sci.* **33** 542
Andersson D 1977 *J. Phys. D: Appl. Phys.* **10** 1549
Anderson K A, Chase L M, Lin R P, McCoy J E and McGuire R F 1972 *Geophys. Res. Lett.* **77** 4611
Anderson L, Ergun R E, Newman D L, McFadden J P, Carlson C W, and Su Y-J 2002 *Phys. Plasmas* **9** 3600
Andrews J G and Allen J E 1971 *Proc. R. Soc. Lond.* A **320** 459
Arefiev A V and Breizman B N 2005 *Phys. Plasmas* **12** 043504
Barkan A and Merlino R L 1995 *Phys. Plasmas* **2** 3261
Beal B E, Gallimore A D, Morris D P, Davis C and Lemmer K M 2006 *Proc. 42nd AIAA.ASME/SAE/ASEE Joint Propulsion Conf. (Sacramento, July 2006)*
Bernstein I B, Greene J M and Kruskal M D 1957 *Phys. Rev.* **108** 546
Biloiu C, Sun X, Choueiri E, Doss F, Scime E E, Heard J, Spektor R and Ventura D 2005 *Plasma Sources Sci. Technol.* **14** 766
Borisov N and Mall U 2002 *J. Plasma Phys.* **67** 277
Boswell R W, Marsch E and Charles C 2006 *Astrophys. J.* **640** L199
Boswell R W and Vender D 1995 *Plasma Sources Sci. Technol.* **4** 534
Block L P 1972 *Earth's Magnetospheric Processes* ed. B M McCormac (Dordrecht: Reidel) p 258
Block L P 1978 *Astrophys. Space Sci.* **55** 59
Brault P *et al* 2004 *J. Phys. D: Appl. Phys.* **37** 3419
Brault P, Roualdes S, Caillard A, Thomann A-L, Mathias J, Durand J, Coutanceau C, Leger J-M, Charles C and Boswell R W 2006 *Eur. Phys. J. Appl. Phys.* **34** 151
Caillard A, Charles C, Boswell R, Brault P and Coutanceau C 2007 *Appl. Phys. Lett.* **90** 223119
Carlqvist P 1982 *Astrophys. Space Sci.* **87** 21
Chabert P, Plihon N, Corr C S, Raimbault J-L and Lichtenberg A J 2006 *Phys. Plasmas* **13** 093504
Chan C, Cho M-H, Hershkowitz N and Intrator T 1984 *Phys. Rev. Lett.* **52** 1782

Chan C, Cho M-H, Hershkowitz N and Intrator T 1986 *Phys. Rev. Lett.* **57** 3050
Chan C and Hershkowitz N 1982 *Phys. Fluids* **25** 2135
Chan C, Hershkowitz N and Payne G L 1981 *Phys. Lett.* **83A** 328
Chang-Diaz F F 2000 *Sci. Am.* **283** 90
Charles C 1990 *PhD Thesis* Orleans University
Charles C 1993 *J. Vac. Sci. Technol.* A **11** 157
Charles C 2004 *Appl. Phys. Lett.* **84** 332
Charles C 2005a *IEEE Trans. Plasma Sci.* **33** 336
Charles C 2005b *Proc. 27th Int. Conf. on Plasmas and Ionized Gases (Eindhoven, July 2005)* Topical 5
Charles C 2005c *Phys. Plasmas* **12** 044508
Charles C *Proc. 6th Int. Conf. on Reactive Plasmas and 23rd Symp. on Plasma Processing (Matsushima/Sendai, January 2006)*
Charles C and Boswell R W 1995a *J. Vac. Sci. Technol.* A **13** 2067
Charles C and Boswell R W 1995b *J. Appl. Phys* **78** 766
Charles C and Boswell R W 1998 *J. Appl. Phys.* **84** 350
Charles C and Boswell R W 2002 *Australian Patent Application Number* 2003232523 (PCT/AU03/00763)
Charles C and Boswell R W 2003 *Appl. Phys. Lett.* **82** 1356
Charles C and Boswell R W 2004a *Phys. Plasmas* **11** 1706
Charles C and Boswell R W 2004b *Phys. Plasmas* **11** 3808
Charles C, Boswell R W, Bouchoule A, Laure C and Ranson P 1991 *J. Vac. Sci. Technol.* A **9** 661
Charles C, Boswell R W and Porteous R K 1992 *J. Vac. Sci. Technol.* A **10** 398
Charles C, Boswell R W and Lieberman M A 2006b *Appl. Phys. Lett.* **89** 261503
Charles C, Costa C, Alexander P, Degeling A, Boswell R and Harris J 1999 *Proc. Australia/Japan/US Workshop on High Performance Computing and Advanced Visualisation in Plasma Physics Research (Magnetic Island, Australia, July 1999)*
Charles C, Degeling A, Sheridan T, Harris, Lieberman M and Boswell R 2000 *Phys. Plasmas* **7** 5232
Charles C, Ramdutt D, Brault P, Caillard A, Bulla D, Boswell R W, Rabat and Dicks A 2007 *Plasma Phys. Control. Fusion* **49** A73
Charles C *et al* 2006a *Proc. 42nd AIAA.ASME/SAE/ASEE Joint Propulsion Conf. (Sacramento, July 2006)*
Chen F F 2006 *Phys. Plasmas* **13** 034502
Coakley P and Hershkowitz N 1979 *Phys. Fluids* **22** 1171
Coakley P, Hershkowitz N, Hubbard R and Joyce G 1978 *Phys. Rev. Lett.* **40** 230
Cohen S A, Siefert N S, Stange S, Boivin R F, Scime E E, Levinton F M 2003 *Phys. Plasmas* **10** 2593
Cohen S A , Sun X, Ferraro N M, Scime E E, Miah M, Stange S, Siefert N and Boivin R F 2006 *IEEE Trans. Plasma Sci.* **34** 792
Conde L, Ibanez L F and Ferro-Fontan C 2001 *Phys. Rev.* E **62** 046402
Conde L and Leon L 1994 *Phys. Plasmas* **1** 2441
Conde L and Leon L 1999 *IEEE Trans. Plasma Sci.* **27** 80
Corr C S, Plihon N and Chabert P 2006 *J. Appl. Phys.* **99** 103302
D'Angelo N 1997 *Phys. Plasmas* **4** 3422
Diebold D, Forest C E, Hershkowitz N, Hsich M-K, Intrator T, kaufman D, Kim G-H, Lee S-G, and Menard J 1992 *IEEE Trans. Plasma Sci.* **20** 601
Dunaevsky A, Raitses Y and Fish N J 2006 *Appl. Phys. Lett.* **88** 251502
Ergun R E, Andersson L, Main D, Su Y J, Newman D L, Goldman M V, Carlsson C W, McFadden J P and Mozer F S 2002 *Phys. Plasmas* **9** 3695
Ergun R E, Su Y J, Andersson L, Carlson C W, McFadden J P, Mozer F S, Newman D L, Goldman M V and Strangeway R V 2001 *Phys. Rev. Lett.* **87** 045003
Esser R, Lie-Svendsen, Janse A M and Killie M A 2005 *Astrophys. J.* **629** L61
Falthammer C-G 2004 *Geofis. Int.* **43** 225
Fruchtman A 2006 *Phys. Rev. Lett.* **96** 065002
Gesto F N 2005 *Master Thesis* Australian National University
Gesto F N, Blackwell B D, Charles C and Boswell R W 2006 *J. Propulsion Power* **22** 24
Goertz C K and Boswell R W 1979 *J. Geophys. Res.* **84** 7239
Goertz C K and Joyce G 1975 *Astrophys. Space Sci.* **32** 165
Gottscho R A, Nakano T, Sadeghi N, Trevor D J and Boswell R W 1991 *SPIE Process Module Metrol. Control, Clustering* **1594** 376
Hairapetian G and Stenzel R L 1988 *Phys. Rev. Lett.* **61** 1607
Hairapetian G and Stenzel R L 1990 *Phys. Rev. Lett.* **65** 175
Hairapetian G and Stenzel R L 1991 *Phys. Fluids* B **3** 899
Halekas J S, Kin R P and Mitchell D L 2003 *Geophys. Res. Lett.* **30** 2117
Hatakeyama R, Suzuki Y and Sato N 1983 *Phys. Rev. Lett.* **50** 1203
Hershkowitz N 1985 *Space Sci. Rev.* **41** 351
Hershkowitz N 2005 *Phys. Plasmas* **12** 055502
Hershkowitz N, Payne G L, Chung Chan and DeKock L R 1981 *Plasma Phys.* **23** 903
Hollenstein C, Guyot M and Weibel E S 1980 *Phys. Rev. Lett.* **45** 2110
Hooper E B 1993 *J. Propulsion Power* **9** 757
Intrator T, Menard J and Hershkowitz N 1993 *Phys. Fluids* B **5** 806
Izuka S, Michelsen P, Rasmussen J J, Schrittwieser R, Hatakeyama R, Saeki K and Sato N 1982 *Phys. Rev. Lett.* **48** 145
Knorr G and Goertz C K 1974 *Astrophys. Space Sci.* **74** 209
Kuhn S 1979 *Plasma Phys.* **21** 613
Johnson J C, Merlino R L and D'Angelo N 1989 *J. Phys. D: Appl. Phys.* **22** 1456
Johnson J C, Merlino R L and D'Angelo N 1990 *J. Phys. D: Appl. Phys.* **23** 682
Keese A M 2006 *PhD Thesis* University of West Virginia
Keese A M, Scime E E, Charles C, Meige A and Boswell R W 2005 *Phys. Plasmas* **12** 093502
Langmuir I 1929 *Phys. Rev.* **33** 954
Levine J S and Crawford F W 1980 *J. Plasma Phys.* **23** 223
Levine J S and Crawford F W 1980 *J. Plasma Phys.* **24** 359
Lieberman M A and Charles C 2006 *Phys. Rev. Lett.* **97** 045003
Lieberman M A, Charles C, and Boswell R W 2006 *J. Phys. D: Appl. Phys.* **39** 3294
Lieberman M A and Lichtenberg A J 1994 *Principles of Plasma Discharges and Materials Processing* (New York: Wiley-Interscience)
Lin R P, Mitchell D L, Curtis D W, Anderson K A, Carlson C W, McFadden J, Akuna M H, Hod L L and Binder A 1998 *Science* **281** 1480
Lindberg L 1992 *Phys. Scr.* **47** 92
Main D S, Newman D L and Ergun R E 2006 *Phys. Rev. Lett.* **97** 185001
Manheimer W M 2001 *IEEE Trans. Plasma Sci.* **29** 75
Meige A 2006 *PhD Thesis* Australian National University
Meige A and Boswell R W 2006 *Phys. Plasmas* **13** 092104
Meige A, Boswell R W, Charles C, Boeuf J-P, Hagelaar G and Turner M M 2005b *IEEE Trans. Plasma Sci.* **33** 334
Meige A, Boswell R W, Charles C and Turner M M 2005a *Phys. Plasmas* **12** 052317
Meige A, Plihon N, Hagelaar G J M, Boeuf J-P, Chabert P and Boswell R W 2007 *Phys. Plasmas* **14** 053508
Merlino R L and Loomis J J 1990 *Phys. Fluids* B **2** 2865
Montgomery D and Joyce G 1969 *J. Plasma Phys.* **3** 1
Newman D L, Goldman M V, Ergun R E and Mangeney A 2001 *Phys. Rev. Lett.* **87** 255001
Ogilvie K W, Steinberg J T, Fitzenreiter R J, Owen C J, Lazarus A J, Farrell W M and Torbert R B 1996 *Geophys. Res. Lett.* **23** 1255
Oksuz L and Hershkowitz N 2002 *Phys. Rev. Lett.* **89** 145001
Parker E N 1958 *Astrophys. J.* **128** 664
Perkins F W and Sun Y C 1981 *Phys. Rev. Lett.* **46** 115
Pike C D and Harrison R A 1997 *Sol. Phys.* **175** 457
Plamodon R, Teichman J and Torven S 1988 *J. Phys. D: Appl. Phys.* **21** 286
Plihon N 2006 *PhD Thesis* Ecole Polytechnique
Plihon N, Chabert P and Corr C S 2007 *Phys. Plasmas* **14** 013506
Plihon N, Corr C S and Chabert P 2005a *Appl. Phys. Lett.* **86** 091501
Plihon N, Corr C S, Chabert P and Raimbault J-L 2005b *J. Appl. Phys.* **98** 023306
Popescu S, Ohtsu Y and Fujita H 2006 *Phys. Rev.* E **73** 066405

Pucci J M, Sinenian N, Palaia J, Celik M, LaBry Z, Shabshelowitz A, Patishchev O and Martinez-Sanchez M 2006 *Proc. 42nd AIAA.ASME/SAE/ASEE Joint Propulsion Conf. (Sacramento, July 2006)*
Quon B H and Wong A Y 1976 *Phys. Rev. Lett.* **37** 1393
Raadu M A 1988 *Astrophys. Space Sci.* **144** 43
Raadu M A 1989 *Phys. Rep.* **178** 25
Raadu M A 1994 *Space Sci. Rev.* **68** 29
Ramdutt D, Charles C, Hudspeth J, Ladewig B, Gegenbach T, Boswell R, Dicks A and Brault P 2007 *J. Power Sources* **165** 41–8
Sato N 1982 *Proc. Symp. on Plasma Double Layers (Roskilde, Denmark)* ed P Michelsen and J J Rasmussen p 116
Sato N, Hatakeyama R, Iisuka S, Mieno T, Saeki K, Rasmussen J J and Michelsen P 1981 *Phys. Rev. Lett.* **46** 1330
Sato K and Miyawaki F 1992 *Phys. Fluids* B **4** 1247
Sato N, Nakamura M and Hatakeyama R 1986 *Phys. Rev. Lett.* **57** 1227
Schrittwieser R, Axnas I, Carpenter T and Torven S 1992 *IEEE Trans. on Plasma Sci.* **20** 607
Shamrai K P, Virko Y V, Virko V F and Yakimenko A I 2006 *Proc. 42nd AIAA.ASME/SAE/ASEE Joint Propulsion Conf. (Sacramento, July 2006)*
Singh N and Khazanov G 2003 *J. Geophys. Res.* **108** 8007
Smith H, Charles C, Boswell R W and Kuwahara 1997 *J. Appl. Phys.* **82** 561
Song B, Berlino R L and D'Angelo N 1992a *J. Phys. D: Appl. Phys.* **25** 938
Song B, Berlino R L and D'Angelo N 1992b *Phys. Scr.* **45** 395
Song B, D'Angelo N and Berlino R L 1991 *J. Phys. D: Appl. Phys.* **24** 1789
Stangeby P C and Allen J E 1973 *J. Phys. D: Appl. Phys.* **6** 224
Sudit I D and Chen F F 1994 *Plasma Sources Sci. Technol.* **3** 162
Sulkanen M E and Borovsky J E 1992 *Phys. Fluids* B **4** 540
Sun X 2005 *PhD Thesis* University of West Virginia
Sun X, Biloiu C, Hardin R and Scime E E 2004 *Plasma Sources Sci. Technol.* **13** 359
Sun X, Keesee A M, Biloiu C, Scime E E, Meige A, Charles C, Boswell R W 2005 *Phys. Rev. Lett.* **95** 025004
Sutherland O, Charles C, Plihon N and Boswell R W 2005 *Phys. Rev. Lett.* **95** 205002
Takahashi K, Charles C, Boswell R W, Kaneko T and Hatakeyama R 2007 Private communication
Tang D and Chu P K 2003 *J. Appl. Phys.* **94** 1390
Taylor R J, Ikezi H and MacKenzie K R 1969 *Proc. Int. Conf. on Quiescent Plasmas (Paris, September 1969)* p 57
Theisen W L, Carpenter R T and Merlino R L 1994 *Phys. Plasmas* **1** 1345
Toki K, Shinohara S, Tanikawa T and Shamrai K P 2006 *Thin Solid Films* **506** 597
Torven S 1979 *Wave Instabilities in Space Plasmas* vol 74 ed P J Palmadesso and K Papadopoulos (Dordrecht: Reidel) p 109
Torven S 1982 *J. Phys. D: Appl. Phys.* **15** 1943
Torven S and Andersson D 1979 *J. Phys. D: Appl. Phys.* **12** 717
Torven S, Lindberg L and Carpenter R T 1985 *Plasma Phys. Control. Fusion* **27** 143
Tu C-Y, Zhou C, Marsch E, Xia L-D, Zhao L, Wang J-X and Wilhelm K 2005 *Science* **308** 519
Verheest F and Hellberg M A 1997 *J. Plasma Phys.* **57** 465
Volwerk M 1993 *J. Phys. D: Appl. Phys.* **26** 1192
Volynets V N, Park W, Tolmachev N, Pashkovsky V G and Yoo J 2006 *J. Appl. Phys.* **99** 043302
Walker R, Bramanti C, Sutherland O, Boswell R W, Charles C, Fearn D, Gonzalez Del Amo J, Frigot P-E and Orlandi M 2006a *Proc. 42nd AIAA.ASME/SAE/ASEE Joint Propulsion Conf. (Sacramento, July 2006)*
Walker R, Chabert P, Plihon N and Raimbault J-L 2006b *Proc. 42nd AIAA.ASME/SAE/ASEE Joint Propulsion Conf. (Sacramento, July 2006)*
Wescott E M, Stenbaek-Nielsen H C, Hallinan T J and Davis T N 1976 *J. Geophys. Res.* **81** 4495
West M, Charles C and Boswell R B 2007 *J. Propulsion Power* Private communication
Williams A C, Weisskopf M C, Elsner R F, Darbro W and Sutherland P G 1986 *Astrophys. J.* **305** 759
Williamson J M and Ganguly B N 2001 *Phys. Rev.* E **64** 036403